The Munali Ni sulfide deposit, southern Zambia: a multi-stage, mafic-ultramafic, magmatic sulfide-magnetite-apatite-carbonate megabreccia

David A. Holwell[*1], Chloe L. Mitchell[1], Grace A. Howe[1], David M. Evans[2] Laura A. Ward[1,3] and Richard Friedman[4].

[1]Department of Geology, University of Leicester, University Road, Leicester, LE1 7RH, UK.

[2]Carrog Consulting, 21 Rue Jean de la Bruyère, 78000 Versailles, France

[3]Carl Zeiss Microscopy Ltd, 509 Coldhams Lane, Cambridge, CB1 3JS, UK

[4]Pacific Centre for Isotopic and Geochemical Research, Department of Earth, Ocean and Atmospheric Sciences, University of British Columbia, 6339 Stores Road, Vancouver, British Columbia, V6T 1Z4, Canada.

*Corresponding author:

Email: dah29@le.ac.uk

Tel: +44 (0) 116 252 3804

Fax: +44 (0) 116 252 3918

Revised manuscript submitted to: Ore Geology Reviews Special Issue – Ni-Cu-PGE Symposium

Abstract

The Munali Intrusive Complex (MIC) is a flattened tube-shaped, mafic-ultramafic intrusion located close to the southern Congo Craton margin in the Zambezi belt of southern Zambia. It is made up of a Central Gabbro Unit (CGU) core, surrounded by a Marginal Ultramafic-mafic Breccia Unit (MUBU), which contains magmatic Ni sulfide mineralisation. The MIC was emplaced into a sequence of metamorphosed Neoproterozoic rift sediments and is entirely hosted within a unit of marble. Munali has many of the characteristics of craton-margin, conduit-style, dyke-sill complex-hosted magmatic sulfide deposits. Three-dimensional modelling of the MUBU on the southern side of the MIC, where the Munali Nickel Mine is located, reveals a laterally discontinuous body located at the boundary between footwall CGU and hangingwall metasediments. Mapping of underground faces demonstrates the MUBU to have intruded after the CGU and be a highly complex, multi stage megabreccia made up of atypical ultramafic rocks (olivinites, olivine-magnetite rocks, and phoscorites), poikilitic gabbro and olivine basalt/dolerite dykes, brecciated on a millimetre to metre scale by magmatic sulfide. The breccia matrix is largely made up of a sulfide assemblage of pyrrhotite-pentlandite-chalcopyrite-pyrite with variable amounts of magnetite, apatite and carbonate. The sulfides become more massive towards the footwall contact. Late stage, high temperature sulfide-carbonate-magnetite veins cut the rest of the MUBU. The strong carbonate signature is likely due, in part, to contamination from the surrounding marbles, but may also be linked to a carbonatite melt related to the phoscorites. Ductile deformation and shear fabrics are displayed by talc-carbonate altered ultramafic clasts that may represent gas streaming textures by CO_2-rich fluids. High precision U-Pb geochronology on zircons give ages of 862.39 ± 0.84 Ma for the poikilitic gabbro and 857.9 ± 1.9 Ma for the ultramafics, highlighting the multi-stage emplacement but placing both mafic and later ultramafic magma emplacement within the Neoproterozoic rifting of the Zambezi Ocean, most likely as sills or sheet-like bodies. Sulfide mineralisation is associated with brecciation of the ultramafics and so is constrained to a maximum age of 858 Ma. The Ni- and Fe-rich nature of the sulfides reflect either early stage sulfide saturation by contamination, or the presence of a fractionated sulfide body with Cu-rich sulfide elsewhere in the system. Munali is an example of a complex conduit-style Ni sulfide deposit affected by multiple stages and sources of magmatism during rifting at a craton margin, subsequent deformation; and where carbonatite and mafic melts have interacted along deep seated crustal fault systems to produce a mineralogically unusual deposit.

Keywords: Magmatic sulfide; Munali; conduit; magmatic breccia; Ni-Cu-PGE; U-Pb dating; carbonatite

63

1. Introduction

The Munali Ni-sulfide deposit is a magmatic sulfide deposit, located in the ultramafic portion of the mafic-ultramafic Munali Intrusive Complex in the Zambezi Supracrustal Sequence, southern Zambia, 75 km south of Lusaka. Sulfide mineralisation is present within an ultramafic megabreccia that surrounds a central, unmineralised gabbro (Evans, 2011). It shares a similar geodynamic setting to a number of other Ni-sulfide deposits in east Africa, emplaced into rifts along the southern margin of the Congo craton during the Neoproterozoic (Evans 2011); consistent with the well-established spatial link between Ni-sulfide deposits and craton margins (Begg et al., 2010; Maier and Groves 2011). Begg et al. (2010) classify Munali as a deposit that is “near” (<100 km) from a craton margin, similar to many other giant deposits, including the similarly aged Jinchuan deposit, China. The central unmineralised gabbro was intruded at 852 ± 22 Ma (unpublished data quoted in Johnson et al., 2007), which constrains its emplacement as a sill-like body into platform sediments during early basin development (Evans, 2011). The mineralised marginal ultramafic unit is interpreted to have been intruded later on simple geological grounds (Evans, 2011), although prior to this study, no geochronology had been performed on this specific unit to determine the absolute timing of mineralisation relative to the central gabbro unit.

The characteristics of the deposit, as a flatted tube-shaped, zoned and composite intrusion with marginal sulfide breccias is typical of many conduit-style magmatic sulfide deposits (Barnes et al. 2016), though we show a significant difference here in that the gabbroic rocks are intruded by a later ultramafic episode of atypical composition. Conduit systems are prime locations for magmatic sulfide mineralisation as they represent areas where processes of crustal contamination (to trigger sulfide saturation), high magma fluxes (to enrich the sulfides in metals) and structural traps (for the accumulation of sulfides) are all operating. These deposits take on a number of morphologies, which may form a continuum: from complex dyke-sill transitions, through tube-like chonoliths into bladed dykes (Barnes et al. 2016). If Munali conforms to one of these models, the timing of emplacement of the marginal ultramafic breccia unit with respect to regional deformation and tilting is critical to distinguishing the deposit as being emplaced as a sill or dyke like body, and determining the direction of sulfide and clast transport and breccia development.

Whilst many models for the emplacement of magmatic sulfide deposits invoke upward transport of sulfide from deeper staging chambers (e.g. Naldrett, 1992; Maier et al, 2011; McDonald and Holwell, 2007; Holwell et al., 2014), there has been a recent recognition that many of the features observed in conduit style deposits, especially sulfide breccia deposits, may be due to the downward movement of sulfide, that may have been generated higher up in the system (e.g. Barnes et al., 2016). Evidence for this lies in the downward penetration of sulfide into footwall rocks along fractures, bedding planes and via partial melting of the floor, exemplified by sulfide breccias in the offset dykes at Sudbury (e.g. Lightfoot and Farrow, 2002; Ripley et al. 2015) and melting of floor rocks at the base of komatiites (e.g. Dowling et al., 2004; Staude et al., 2016). In steeply dipping intrusions, the migration of sulfide within the magma body may be significant and sulfide accumulations may have formed above the current level of erosion and been transported as late stage slurries down the margins of intrusions due to gravity, or late-stage 'draw-back' (Barnes et al. 2015; Hughes et al. 2016).

This paper presents the first comprehensive field study of the nature of the Munali Ni-sulfide deposit, by way of detailed underground geological mapping and observations from drillcore. We demonstrate, from a combination of first order field relationships with supporting 3D lithological modelling, geochronological data, and petrographic and mineralogical observations, the complex geological history of the complex and in doing so provide the first robust geological framework for a genetic model for the deposit.

2. Regional geological setting

The Munali Intrusive Complex (MIC) is situated within the Zambezi Supracrustal Sequence (ZSS), which lies within the medium- to high-metamorphic grade Zambezi Belt, located between the southern margin of the Congo-Tanzania-Bangweulu craton and the northern margin of the Zimbabwe craton (Fig. 1A). The ZSS overlies a basement complex of gneisses and granites of the 1106 Ma Mpande Gneiss (Hanson et al. 1988) and the 1090 Ma Munali Hills Granite (Katongo et al., 2004) which represent the oldest rocks in the area. The ZSS itself is made up of a sequence of early Neoproterozoic sedimentary, volcanic and volcaniclastic rocks that may represent a full tectonic cycle of continental rifting, opening and subsequent closure of the Zambezi Ocean and subduction metamorphism (John et al. 2003; Katongo et al. 2004; Johnson et al. 2007). Overlying the basement complex, the oldest volcano-sedimentary units are the metavolcanic rocks of the Kafue Rhyolite Formation and phyllites of the Nazingwe Formation, which are exposed to the south and east of Kafue (Fig. 1B). Overlying these are marbles, quartzites and pelites referred to as the Mulola and Chipongwe Formations to the north and east of Kafue, and as the Nega Formation to the south and west of Kafue, in the Munali area (Fig. 1B). These predominantly clastic sedimentary rocks are overlain by marbles and calc-silicate rocks of the Cheta or Muzuma Formations (Fig. 1B).

Geochronological work by Johnson et al (2007) constrained the timings of a number of events in the region, including the maximum age for the deposition of the Nega Formation, which was deposited unconformably on top of the basement Munali Hills Granite and Mpande Gneiss after ~1090 Ma. The Kafue Rhyolite Formation at base of the Nega Formation, is now dated at ~880 Ma and is interpreted to coincide with the onset of continental rifting (Hanson et al., 1994; Johnson et al., 2007). There are a number of later felsic igneous intrusions in the region, including the Ngoma Gneiss (~820 Ma), which are interpreted to have been emplaced following the main phase of sedimentation within the rift basins and thus give an upper limit of basin sedimentation in the early Zambezi Rift.

During rifting, intra-plate magmatism occurred that was, in southern Zambia, mostly manifest by mafic igneous intrusions emplaced into high level basin sediments (Evans, 2011). This included the intrusion of the Munali gabbro into sediments of the Nega Formation at ~852 Ma (unpublished data cited in Johnson et al. 2007). Scattered outcrops of eclogitic gabbro extending in an arc to the north of the Kafue River have been interpreted to represent fragments of the putative Zambezi Ocean (John et al. 2003), with eclogite facies metamorphism occurring at ~595 Ma, recording the timing of subduction of the ocean basin to ~90 km. All units were deformed and metamorphosed during the Late Neoproterozoic Pan African event, which affected southern Zambia between 550 and 520 Ma (Porada and Berhost, 2000; Goscombe et al., 2000; Johnson et al., 2005; Bingen et al. 2009), imparting greenschist to amphibolite-grade metamorphism on the sediments and mafic intrusions during the final Congo-Kalahari collision.

2.1 Host rocks to the Munali Intrusive Complex

The MIC is located along the southern flank of the Munali Hills (Fig. 2), and is hosted by a sequence of metasedimentary rocks that are part of the ZSS. Northeast of the MIC, basement rocks of the Munali Hills Granite make up the core of the Munali Hills, which is overlain by a sequence of biotite-kyanite schists and hematitic quartzite and conglomerate at the base of the Nega Formation (Johnson et al. 2007). A major crustal lineament, the Munali Fault, has been inferred from geophysical data and this lies immediately to the northern edge of the MIC (Fig. 2). The intrusive complex is entirely hosted within a marble at the base of a highly variable unit of marble, calc-silicate, cherty quartzite, graphitic biotite-garnet and biotite-scapolite schists and carbonate-bearing hematitic quartzite, which is overlain to the southwest by a thick, monotonous sequence of biotite and biotite-andalusite schists of the Upper Nega Formation (Fig. 2). The biotite-kyanite schists to the northeast of the Munali fault seem to represent a significantly higher metamorphic grade than the biotite and biotite-andalusite schists to the southwest, implying significant movement on the fault (possibly SW-directed thrusting) to juxtapose two terranes of significantly different metamorphic grade. The presence of abundant scapolite, especially in the variable marble unit is thought to be due to the former existence of evaporites in the sequence (Hanson et al., 1994), that have since been removed by diapirism or replaced during metamorphism (Evans, 2011).

2.2 The Munali Intrusive Complex

The MIC is made up of two main units (Fig. 2): the Central Gabbro Unit (CGU) and the Marginal Ultramafic-mafic Breccia Unit (MUBU). The only previously published work on Munali comprises a short description of the setting and nature of the deposit in Evans (2011). He described a relatively undifferentiated, but fine-coarse grained gabbroic core (the CGU) and an ultramafic marginal breccia with textures suggestive of vigorous transport of molten sulfide with silicates in a confined channel (the MUBU). Evans (2011) made comparisons with Voisey's Bay, and Aguablaca in terms of the emplacement of sulfide in conduit settings. The MUBU is a coarse, brecciated, dominantly ultramafic unit with sulfide, magnetite, apatite and carbonate. It shows an intrusive relationship with the CGU and includes barren olivine dolerite with quench textures. The mineralised MUBU dips very steeply to the southwest and is present on both the northeastern and southwestern flanks of the CGU, though there is no evidence from surface exposure or drillcore available of a connection between the two flanks . The southwestern margin has the thickest MUBU, up to a few tens of metres and comprises three main zones of mineralisation from southeast to northwest: Enterprise (the site of the Munali Nickel mine), Voyager and Intrepid (Fig. 2). Evans et al. (2006) originally suggested that the mineralisation style was intermediate between magmatic sulfide and skarn mineralisation, but later suggested a stronger magmatic origin, with sulfides derived from relatively high-Mg basaltic or picritic magmas (Evans, 2011).

A U-Pb SHRIMP zircon crystallization age of 852 ± 22 Ma has been reported for the CGU (unpublished data cited in Johnson et al. 2007) though no dating has been attempted on the MUBU prior to this study. This age places the Munali gabbro as being emplaced into platform sediments during extension and rifting along the margins of the Congo craton, presumably as a sill like body. Johnson et al. (2007) and Evans (2011) both suggest that the MIC was part of the early extensional magmatism along the Katanga Rift, related to the breakup of Rodinia. Evans (2011) suggested a similar setting for the formation of three other Ni sulfide deposits in east Africa; Mpemba in Malawi, Rovuma (the Cabo Delgado nickel belt) in Mozambique, and Nachingwea in Tanzania. Whilst the emplacement age of the gabbro implies its injection as a sill, the sulfide-bearing MUBU is younger, based on geological observations of cross cutting relationships (Evans, 2011). As such, it may represent a related sill like injection, or a much later dyke intruded along the same conduit, but after regional tilting. The geological model of emplacement relies critically on this distinction.

2.3 Exploration and mining history

The Munali Ni-sulfide deposit was discovered by a regional geochemical stream survey by Chartered Exploration Ltd. in 1969, which was followed up by exploration and resource definition work by Anglo American Corp. between 1970 to 1977. Sporadic exploration, including trenching over some of the gossans, took place up until the 1990s by a number of companies including Apollo Mining Ltd and Murchison Exploration. In 2002, Albidon Ltd began an extensive program of exploration, including a major diamond drilling campaign around the MIC, and regional exploration of several prospective targets along strike. A Bankable Feasibility Study was completed in 2006 and Albidon announced it would commence construction of a mine on the Enterprise deposit (Albidon 2006), which opened in 2008. The mine encountered a range of financial, metallurgical and management problems and was put on care and maintenance in 2011. In 2014 the Jinchuan Group purchased Albidon Ltd. outright, and under a lease agreement, Consolidated Nickel Mines (CNM) took over operations in the same year through their wholly-owned Zambian subsidiary Mabiza Resources Ltd. The mine has undergone a revised Feasibility Study, a new geological model has been developed, a new JORC resource has been defined (total measured and indicated resources of 5.6Mt at 1.01% Ni at a cut-off of 0.6% Ni) and a new mining method has been planned (CNM, 2016).

3. Sampling and methods

3.1 Fieldwork

Samples of representative igneous rocks and sulfide textures were taken from exploration drillcore from the Enterprise, Voyager and Intrepid mineralised zones. Quarter core samples of lengths 15-25 cm were collected from several drillholes, the collar locations of which are marked on Figure 2. Underground mapping was undertaken on three cross cuts on three levels (level, 870, 845 and 820) of the Enterprise mine; two footwall access drives that expose the main footwall contact on the 845 and 820 levels; and two strike-parallel sections along the footwall drive on the 845 and 820 levels. This first use of detailed lithological underground mapping at the mine enabled better visualisation and interpretation of intrusive relationships between mineralisation styles compared with logging drill cores, especially given the coarsely heterogeneous nature of the deposit. Cross cuts were chosen to intersect the thickest portion (~40 m) of the MUBU, so as to provide as much geological information as possible across a single section.

3.2 3D modelling

Drillhole data provided by Mabiza Resources Ltd. was modelled in 3D space using Micromine 2014 software in order to constrain the subsurface morphology of the MUBU, and is presented in Section 5. Drillhole traces were displayed by simplifying downhole lithology data to display three lithological units: the metasedimentary hangingwall, the MUBU and the CGU. Micromine's implicit modeller was then used to extrapolate the intersection surfaces between these three units to create a 3D model of the MUBU along the southwestern margin of the MIC.

3.3 Mineralogy and petrology

Thirty samples were selected for thin sectioning for petrological and mineralogical analysis at the University of Leicester. Olivine compositions were determined at the University of Leicester using a JEOL 8600 Superprobe with a wavelength dispersive system, fitted with an Oxford Instrument ED Spectrometer using Aztec software. A 30 nA current, 15 kV accelerating voltage and 5 µm beam diameter were used for all analyses. Samples containing zircons for geochronology were mapped at ZEISS's Natural Resources Laboratory in Cambridge, UK, using the Mineralogic Mining software and petrological analyser. A ZEISS Sigma VP field emission scanning electron microscope (SEM) coupled with two Bruker 6 | 30 Energy Dispersive X-ray (EDX) Spectroscopy detectors was used. A mapping analysis was selected with a step size of 10 microns. Samples were analysed using an acceleration voltage of 20 keV at a working distance of 8.5mm. Counts for EDX detection were consistently above 3000 with mineral classifications based on stoichiometric values. EDX calibrations were performed every hour on a Cu standard to normalise the beam alongside a brightness and contrast calibration to help limit the effects of beam drift. Thin section photomicrographs collected using the ZEISS Imager Z2N light microscope and Mineralogic maps were layered and visualised using the ZEISS Atlas correlative software.

3.4 U-Pb geochronology

Samples of coarse poikilitic gabbro and ultramafic pegmatite were collected from diamond drill core MAD036 (at 155 and 216 m, respectively). Zircons were identified in thin section using Zeiss's automated Mineralogic Mining Software. Zircons were separated from the samples using conventional crushing, grinding, wet shaking table, heavy liquid, and magnetic separation methods at the Pacific Centre for Isotopic and Geochemical Research, University of British Columbia, Canada. All analytical procedures and methods for the Chemical Abrasion-Thermal Ionisation Mass Spectrometry (CA-TIMS) technique used in this study were followed from those described in detail in Mortensen et al. (2015). Final ages assigned to the samples dated in this study are based on weighted averages of four individual $^{206}Pb/^{238}U$ ages from concordant single grain analyses. Age uncertainties are reported at 2σ level.

4. Field relationships

4.1 Surface outcrop

The MIC is lozenge shaped in surface outcop: 2.6 km long in the NW-SE orientation and up to 600 m wide (Fig. 2). The complex is located in a topographic low, bounded to the north by the Munali Hills, and to the south by a thin, discontinuous ridge of metasedimentary rocks of the Lower Nega Formation, beyond which, the pelitic Upper Nega Formation makes up a flat arable plain (Fig. 3). The intrusion and the host rock metasediments dip steeply to the SW (Fig. 2). The Munali Hills are largely comprised of granitic and gneissic basement rocks, and bordered by a series of interlayered high grade biotite-kyanite schists and hematitic quartzites to the northeast of the inferred Munali Fault (Fig. 2). To the southwest of the fault, the intrusive rocks are entirely enclosed by a marble unit of the Lower Nega Formation. The marble shows strong cm-scale layering, is blue-grey in colour (Fig. 4A) but becomes white towards the contact with the igneous units, and contains abundant pyrite (Fig. 4B,C). Layering in the marbles and other country rock units dip consistently and steeply (70-80°) to the southwest (Fig. 2). Outcrop mapping shows that the marble bends to accommodate the intrusion, and has a smaller net thickness in the area of the intrusion, indicating that the emplacement of the MIC both created space, which it infilled, but also assimilated some of the country rock host (Figs. 2,3). Alternatively, it may be due to structural thinning around the more rigid igneous body during later deformation. To the southwest of the marble outcrop (up-stratigraphy), the remainder of the sequence on the area is composed of thin graphitic and garnet-bearing schists, thin marble interbeds, a carbonate-rich hematitic micaceous quartzite of the lower Nega Formation, and thick biotite and biotite-andalusite schists of the Upper Nega Formation, shown well in drillcore (Fig. 4C).

The CGU is composed of heterogeneously textured, magnetite-bearing ophitic to subophitic gabbro (Fig. 4D). Outcrops are sparse, except in the northwestern sector of the intrusion where a few small hills have exposures of coarse and medium-grained gabbro and plugs of dolerite (Fig. 4E). Contacts between these different textured gabbros are not exposed at surface but may represent multiple stages of intrusion rather than layering. Some disseminated pyrite is present within the gabbros, mostly related to cross-cutting carbonate veins. All these rock types have been subject to greenschist facies metamorphism (uralitic, scapolitic and epidotitic alteration), but their igneous textures have been largely preserved.

The MUBU, which hosts the sulfide mineralisation, is poorly exposed along the southwestern and northeastern margins of the complex. It is important to note at this point that whilst the mineralisation is hosted within the MUBU, the volumes of sulfide along strike and downdip vary greatly, and the MUBU itself is a lithological unit containing mineralised zones, and is not, in itself, an orebody. Four main gossans are present (Fig. 2); three of which are along the southwestern margin: in the south at Enterprise, in the central part of the complex at Voyager; and on the top of a prominent, hill at Intrepid (Fig. 3B, 4F). A small gossan is also present in the northwestern part of the northern margin at Defiant (Fig. 2). These units do not entirely enclose the gabbro, and form two parallel strips along either side of the gabbro (Figs. 2,3). The gossans indicate that the MUBU on the southwestern margin is thicker (40 to 100m at surface) and better developed, and that the continuity of mineralisation at the surface may be variable. The gossans are comprised of breccia blocks of highly-weathered gabbroic and ultramafic lithologies elongated parallel to the contact within a strongly ferruginous matrix (Fig. 4F). Although the gossan outcrops are not continuous, soil sampling and trenching on the southwestern margin shows that the MUBU is continuous at surface, but contains widely varying sulfide contents. The northeastern marginal unit is thinner, but trenching and some drilling has also shown it to be consistently present along this margin. Both MUBU bodies, and the CGU, dip steeply to the southwest, concordant with the host rock sedimentary layering. The thicker, southwestern MUBU therefore has metasediments as its hangingwall, and the CGU as its footwall. In the following sections, we concentrate on this unit and therefore 'footwall' always refers to the CGU along the southwestern flank of the MIC.

Although the MUBU is predominantly ultramafic, especially in the most mineralised portions, it is also comprised of variable amounts of poikilitic gabbro and olivine dolerite/basalt, which are described in more detail below. Furthermore, a variety of hybrid lithologies formed from the mixing of mafic or ultramafic magmas with assimilated country rock marble and schist are present, particularly towards the hangingwall contact. Contacts with adjacent rock types are rarely observed at surface, but can be examined in detail in drill cores. The outer contact with the marbles is diffuse over a few centimetres and is marked by a zone of hybridised rock made up of carbonate, hydrous mafic minerals, and minor magnetite and sulfide or takes the form of a carbonate-veined metadolerite (Fig. 4C). The inner contact with the CGU is marked at surface by the relatively abrupt transition from gossanous breccia to a homogenous microgabbro lithology over the space of several metres.

4.2 Underground face mapping

The MUBU-hosted orebody at Enterprise has been mined down to the 820 level; some 275 m below the surface. The underground workings follow the steep, sulfide-rich footwall contact where the MUBU is in sharp contact with the CGU footwall and allows for examination of the footwall contact as strike parallel sections in the backs or northeastern faces of the main footwall drive (e.g. those shown in blue in Figure 5), or as cross sections in the access drives (e.g. those shown in green in Figure 5). The MUBU thickens out from around 7 m at the surface to over 40 m at the 870 level, and several cross cuts expose sections through the orebody at these levels (Fig. 5). Figure 6A-C shows mapped sections of cross cuts on the 820, 845 and 870 levels, respectively (shown in red in Figure 5), demonstrating the nature of the orebody in section on a metre to decimetre scale in its thickest zone and clearly showing the coarsely heterogenous, megabreccia nature of the deposit. The sections shown in Figure 6 stop short of showing the footwall contact to the northeast as this has been largely removed by mine development. However, the contact is visible in some of the access drives, which cut through the footwall into the orebody. Figure 7 shows two examples of the footwall contact in detail in section from the access drives, and Figure 8 shows two strike-parallel sections of the footwall (northeastern) side of the main footwall drive, where the footwall contact is exposed part way up the face.

The basal contact of the orebody with the unmineralised CGU footwall is variable and can be sharp (Fig. 8C,D), but in many places sheeted veins of massive sulfide and talc-carbonate altered ultramafic material intrude the gabbro footwall sporadically within a zone up to 15 m from the contact proper (Fig. 7). This variability is encountered in drill core, with some cores containing no sulfide below the main footwall contact, but many showing sulfide veins sporadically intruding the gabbro for several metres. These footwall veins, where present, are commonly parallel to the main contact, though there are frequent examples of sulfide veins in all orientations (Figs. 7, 9A,B,C) and evidence of cross cutting sulfide-bearing phases (Fig. 9C). The main footwall contact is often marked by a thin (5-10 cm) zone of talc-altered material with apatite and sulfide (Fig. 7A,B, 9A). Figure 9A shows the footwall contact in detail and Figures 9B and C show sulfide injection into the first few metres of the footwall. In Figure 9A, the footwall contact is marked by a massive sulfide vein, which cuts down vertically into the footwall gabbro. The injection of sulfide into the floor clearly shows that sulfide injection occurred into solid gabbro. A zone of talc-carbonate altered clasts appears to show a sheared fabric at the contact with the massive sulfide (Fig. 9A).

We define the footwall contact as being the point where the igneous rock changes from gabbro (footwall) to ultramafics, poikilitic gabbro or olivine dolerite/basalt (Fig. 7,8). The footwall contact that is exposed in the access drive of the 820 Level (Fig. 7C,D) displays a 5 metre zone of highly brecciated gabbro with mostly massive sulfide matrix below the main contact. Similar textures are also seen in the strike-parallel sections shown in Figure 8. The sulfide ingress into the gabbro does not have a preferred orientation, and does not represent sheeted veins in this case.

Underground exposures in the backs of the footwall drive show some metre-scale, along-strike continuity of sulfide and talc-carbonate altered ultramafic sheets shown in Figure 7, which contrasts to the more random brecciation seen away from the contact in Figure 6, though the 820 Level (Fig. 6C) does show several dykes and sulfide-bearing bodies aligned with the steep southwesterly dip. As such, closer to the footwall contact, there is more along-strike continuity in what appear to be sheeted injections of sulfide, ultramafic and talc-carbonate bodies (Fig. 7), which give way to a more chaotic brecciated nature in the main part of the MUBU (Fig. 8), before progressing to dominantly hybrid lithologies at the hangingwall contact (Fig. 4C). In general, the volume of sulfide in the orebody increases towards the footwall contact (Fig. 8). Furthermore, the clast content of the sulfide component increases away from the footwall contact such that the sulfide portions grade from massive to semi massive to patchy away from the footwall contact.

A key relationship revealed by the underground mapping is the clearly coarsely heterogeneous, megabreccia nature of the orebody shown particularly in Figure 6. Variable proportions of sulfide, oxide, apatite and carbonate make up the matrix of the breccia and several stages of sulfide injection/association are recognised that cross cut each other (Fig. 6,7,8; Fig 9C), and infill the space between igneous rocks and clasts. The different sulphide stages are described in more detail below. The clasts are composed of ultramafics (Fig. 9D), mostly unusually coarse olivine cumulates with variable amounts of magnetite±apatite in them, and poikilitic gabbro. Our mapping has identified that the poikilitic gabbro is the dominant igneous rock type (clast) in the upper levels and ultramafic clasts are more common in the lower levels of the mine (Fig. 6), however at all levels there are examples of both juxtaposed against each other (e.g. Fig. 9E), illustrating some transport of the clasts. Many clasts show magnetite reaction rinds against the sulfide, typically 1-2 cm thick, irrespective of clast composition (Fig. 9E).

The olivine dolerite/basalt dykes are generally aligned roughly parallel to the main footwall contact (Fig 6). However, they are brecciated and injected by sulfide and talc-carbonate material (Fig. 6; Fig 9F), but only to a moderate degree so as to retain an apparently original orientation. As such, they are considered to be close to their in situ emplacement position, and have been affected by some late stage brecciation and sulfide injection, but are not as significantly disrupted as the ultramafics appear to be. Thus, we interpret the injection of the olivine dolerite/basalt to postdate the ultramafic intrusion, but not the sulfide breccia

The ultramafics are present as clasts on a scale of several metres, down to a centimetre scale in the faces mapped. They are, however, seen to intrude the gabbro in core – see below – and other parts of the mine. Some of the clasts are barren of sulfide mineralisation, but some contain interstitial sulfides and magnetite. As such, there is evidence of sulfide formed during crystallisation of the ultramafics, and later infiltration of sulfide during fracturing of the clasts and breccia formation. On level 845 (Fig. 6), the ultramafic shows an interfingering relationship with the olivine dolerite, though with a serpentinised reaction rim (Fig. 9G). This may have originally been a pyroxene/amphibole (tremolite) reaction rim, between calcic basalt and the olivine. This is one of the rare occurrences where the relative timing between ultramafic and olivine dolerite/basalt can be observed and suggests intrusion of dolerite into the ultramafic with the reaction zones in the ultramafic indicating they may not have been in equilibrium and may have different sources. Similar relationships observed in core suggest that the dolerite intrudes the ultramafic, with the latter becoming highly altered at the contacts (Fig. 10A) and this is consistent with the above observation of relative disruption by brecciation implying a later stage emplacement for the dykes.

Throughout the orebody, white clasts of talc-carbonate-altered ultramafics are present within what appear to be ductile, sheared or 'fluidised' zones with massive sulfide matrix. These textures are present in discrete zones within the orebody, commonly along strike-parallel structures, though they are anastomising and can be found in all orientation (Fig. 6; 9H). The clasts are composed of talc and magnesite and appear to be highly fluid altered clasts of originally ultramafic composition.

A number of faults run through the Munali orebody and are exposed underground. These are almost all sub-parallel with the intrusion margins and are either syn-emplacement and/or post emplacement. Fault planes dip steeply to the southwest and are apparently normal faults (evidence from fault drag; Fig 9I). Absolute offsets are large enough not to be traceable in the underground faces and are, therefore >5 m. Due to the brecciated nature of the orebody, any oblique movement on the faults would make correlation in the vertical faces impossible to define. Fault planes are generally highly serpentinised and/or replaced by talc and carbonate and contain sulfide (Fig. 6,9I).

4.3 Other key relationships observed in drillcore

Intrusion of the ultramafic melts into the gabbro is exemplified by intersections from drillhole MAD189A from Voyager (Fig. 2), where ultramafic rocks cross cut altered gabbro (Fig. 10B) and in places contains clasts of altered gabbro (Fig. 10C), clearly showing the ultramafic rocks as being intruded after solidification of the gabbro. A further cross cutting relationship that has been constrained from core observation is that dykes of olivine basalt/dolerite are seen to intrude the poikilitic gabbro (Fig. 10D) as well as the ultramafics (Fig. 10A). The relationship shown in Figure 10A shows the basalt interpenetrating and disaggregating the olivine cumulate, along grain boundaries, and also the universal reaction rim on olivine against the basalt.

Figure 10E shows a thin olivine basalt dyke containing an angular clast of massive sulfide, intruded into poikilitic gabbro, with magnetite reaction rinds along the margins. As such, whilst the olivine basalt is clearly post-poikilitic gabbro, there is evidence of some sulfide present prior to the intrusion of the olivine basalt, which again is consistent with the observations in the underground faces that the olivine basalt intrusions have only undergone a relatively minor amount of brecciation and sulfide intrusion and were emplaced after the initial stages of sulfide injections.

5. 3D modelling

Assessment of drillcores from the entire strike length of the intrusion reveal that the MUBU is not as continuous at depth as it is at the surface. Due to the lack of outcrop in places, the inference of a continuous MUBU in the surface mapping (shown in Figure 2) may not be correct and the information from the drillcores indicates a much more inconsistent thickness along strike. Away from the Enterprise deposit, the drillcore information indicates the MUBU (where present) consists of similar mixed lithologies of poikilitic gabbro, ultramafics, olivine dolerite dykes and massive to semi-massive sulfide breccia fills. As such, the MUBU us mapped in the Enterprise mine and shown in Figures 6-8 can be broadly considered representative of the unit as a whole across the southern flank of the MIC, though the amount and proportions of each of the constituent rock types varies along strike. Deep drilling in the far southern tip of the MIC, and in several sections along strike intersect gabbro in direct contact with the country rock marble, with little or no ultramafic or mineralised rocks. However, down dip of the Enterprise mine, even the deepest drillholes (MAD068, 182, 184; Fig.2) intersect MUBU, and as such, the down dip extent of the mineralisation has not been intersected in this area.

To visualise this and the subsurface morphology of the MUBU along the southwestern margin of the intrusive complex, drillcore information from the historical exploration drilling programs was used to construct a 3D model of the MUBU using implicit modelling in Micromine software. Drillholes used in the model are shown in Figure 11A. The northeastern marginal unit was not modelled due to the much smaller number of drillholes intersecting this unit meaning the implicit modelling would be restricted. Drill hole traces were displayed to show intersections with either the metasedimentary rocks of the Nega Formation, the MUBU (ultramafic rocks, poikilitic gabbro, olivine dolerite and massive/semi massive sulphides), or the CGU. In this case, the modelling involves the interpolation of lithological contacts to create open or closed surfaces in 3D space. As such, the resultant model shows a lithological unit (the MUBU), and does not represent an ore grade shell.

The results of the 3D modelling are shown in Figure 11B-D. The model shows that the MUBU is a discontinuous, NW-SE trending body with a steep dip to the southwest (Figs. 11B,C), with its thickest and most consistent zone at Enterprise. The surface gossans (Fig. 11A) correspond to parts of the breccia unit that extend up to the surface (Fig. 11B). At the very southern tip of the intrusion, the MUBU bottoms out at ~300 m towards the edges of the model where drill holes intersect metasedimentary country rocks at depth in direct contact with the CGU. However, beneath the Enterprise mine itself, the deepest holes intersect the MUBU at depths of 690 m, potentially indicating continuation of the MUBU down dip (Fig. 11B-D). Other areas where the base of the unit has not been proven include a deep zone between Voyager and Enterprise, and three zones under Intrepid, in the north. The results of this modelling indicate that whilst the CGU is a consistent body down dip and along strike (Fig. 11A), the MUBU represents a more complex network of anastomosing intrusions emplaced along the contact between the gabbro and the hangingwall and the metasediments.

6. Petrology of the igneous host rocks

6.1 Central gabbro unit

The CGU is a variably textured gabbro, from microgabbro (Fig. 12A), which makes up the typical footwall to the mineralised MUBU along the southern flank, to areas of coarser grained gabbro which are exposed at the surface in the northern part of the intrusion at the gabbro hills (Figs. 2,3). Plagioclase crystals have no preferred alignment, are euhedral with growth zoning and clouded by very fine needle-like inclusions of Fe-oxides and are altered to scapolite on their margins. Clinopyroxene is subhedral to anhedral, occupying interstitial positions relative to plagioclase and is generally altered to secondary amphiboles (actinolite) and chlorite (Fig. 12A,B). The gabbros contain magnetite, ilmenite and some minor apatite and pyrite (Fig. 12B).

6.2 Poikilitic gabbro

Poikilitic gabbro is present around the marginal part of the CGU and is a major constituent of the MUBU, compositionally similar to the CGU and made up of euhedral plagioclase (2-15 mm) chadocrysts, with clinopyroxene and magnetite oikocrysts (Fig. 12C,D). Similar poikilitic gabbro with well-aligned trachytoidal plagioclase laths have been observed within the main mass of the CGU, interlayered with more gabbros with more randomly oriented plagioclase. Plagioclase chadocrysts are mostly randomly arranged (Fig. 12D) other than in the aforementioned trachytoidal rocks. The plagioclase also contains a very fine dusting of needle or platy Fe-oxides that give a brownish cloudy tinge to the feldspar. The oxides display exsolution from magnetite of both coarser intergranular ilmenite and crystallographically oriented lamellae of ilmenite. Clinopyroxene is altered to actinolite (Fig. 12D). Sulfides are rare but where present are comprised of pyrrhotite-pentlandite-chalcopyrite blebs present interstitial to the plagioclase laths.

6.3 Ultramafic rocks

The ultramafic at Munali are atypical of most ultramafic-hosted Ni sulfide deposits. The rocks are dominated by coarse to very coarse grained, rounded to subhedral olivine (mostly partly or wholly serpentinised or altered to talc-carbonate) in a meso to adcumulate texture. The olivine is always whole, has rounded to subhedral, annealed textures, and is not skeletal, indicating slow growth. In addition to olivine, there are variable amounts of ilmenite-magnetite, apatite, and very rare clinopyroxene. A particularly unusual characteristic of Munali is that no chromite is present in any of the ultramafic rocks. The most common rock type is a serpentinised olivinite with minor magnetite +/- sulfides (Fig. 12E,F). The term olivinite is used here rather than dunite, reflecting the oxide phase as being magnetite rather than chromite. Very rare pegmatitic wehrlites (the only ultramafic to contain any clinopyroxene) also occur, containing interstitial magnetite-sulfide-apatite (Fig. 12G). Many of the olivinites contain interstitial aggregates of pyrrhotite-pentlandite-chalcopyrite-magnetite-apatite that can make up a few modal % of the mineralogy (Fig. 12H). The presence of olivine with apatite and magnetite such that olivine makes up less than 90% of the rock would allow a classification of such rocks as phoscorites. The co-existence of magmatic sulfide alongside the apatite and magnetite (Fig. 12H) with phoscorites is highly unusual. The proportion of magnetite in the ultramafic rocks varies, with some olivine-magnetite rocks commonly containing up to 50 modal% magnetite (Fig. 12I).

The vast majority of olivines have been completely serpentinised in these rocks, however, a limited number of fresh olivine grains were identified and compositions are reported in Table 1. Olivines from the olivinites have Fo contents in the range 81.2 to 83.2, with Ni contents of up to 1154 ppm (mean: 610 ppm; Table 1). In the olivine-magnetite rocks, and a sample of pegmatitic wherlite, the Fo contents of the olivine are lower (~77), but the Ni is very similar (Table 1). Evans (2004) reported olivine from an adcumulate olivinite to have core compositions of Fo_{77} to Fo_{79} with Ni about 600-900 ppm, and rim compositions of Fo_{79} to Fo_{82}, Ni = 600-1000 ppm.

6.4 Olivine basalt/dolerite

Olivine basalt (and texturally also dolerite) occurs as dykes and thin intrusions identified mostly within the MUBU (Fig. 12J). They are moderately disrupted by the brecciation (Fig. 9F). These rocks are often susceptible to alteration due to their fine grain size (Fig. 12K), but this is not usually accompanied by strain/deformation. In the least-altered basalts, the groundmass is formed by abundant small, randomly-orientated plagioclase laths with a scalloped-margin texture, with intergranular clinopyroxene (Fig. 12K). Olivine forms subhedral to euhedral hopper phenocrysts that are always altered to dark green-brown serpentine (Fig. 12K). There may be lesser pyroxene phenocrysts, now replaced by aggregates of colourless tremolite-actinolite. The skeletal and hollow texture of olivine phenocrysts can still be recognised in less-altered samples. Alteration assemblages are mostly poikiloblastic scapolite for plagioclase, and actinolite for intergranular clinopyroxene. This rock type characteristically contains very little magnetite and no sulfides, other than as clasts (Fig. 10E) or as fracture fills.

7 Sulfide mineralisation

Five distinctive textural styles of sulfide have been identified. In all cases, the sulfide mineralogy is made up of pyrrhotite>>pentlandite>chalcopyrite±pyrite with magnetite making a small, but ubiquitous component of all the sulfide assemblages. Bulk tenors of the ores are ~2-3% Ni, 0.2-0.3 % Cu and < 3 ppm Pt+Pd (Mitchell, 2016). The styles defined based on texture and associated mineralogy are:

1. Massive sulfide breccia fills, veins and injections
2. Massive sulfide-apatite-magnetite breccia fills and veins
3. Massive sulfide with sheared and talc-carbonate altered clasts
4. Carbonate-sulfide-magnetite veins
5. Disseminated interstitial sulfides in ultramafic and poikilitic gabbro rocks.

A full geochemical and mineralogical study of the sulfides is out of the scope of this paper and will be presented elsewhere. Here we describe the textural relationships and significance with regards to our detailed chronological timeframe.

7.1. Massive sulfides

The majority of the orebody is made up of breccia fills and veins of massive or semi-massive sulfides (Figs. 6,7,8,9,13A). Igneous rock clasts within the breccia have a range of shapes from angular (Fig. 13A) to sub rounded on scales from a few millimetres (Fig. 13D) to metres (Figs. 6-8). The sulfides are composed largely of pyrrhotite, with pentlandite cell textures and small, rarer patches of chalcopyrite (Fig 13B,D). Magnetite is ubiquitous as a minor phase and pyrite is present sporadically. Euhedral apatite crystals, up to 30 cm in size are common in some areas (Fig. 13C,D), though its presence appears to be characteristic of some, but not all injections of massive sulfide, implying a multi-stage emplacement history of sulfide liquids. The apatite-bearing massive sulfides also have a higher (<20 modal %) proportion of magnetite (Fig. 13D). Some massive sulfides are associated with clasts of talc-carbonate (magnesite) altered ultramafics (Fig. 13E). These are common in the more sheared parts of the orebody. Cross cutting relationships indicate that the shearing is later than the massive sulfide veins (Fig. 9C). Notwithstanding this, the assemblage of the sulfide portion remains consistent with the other massive sulfide veins.

7.2 Carbonate-sulfide-magnetite veins

These irregular veins and patches are late in the paragenesis, cross cut many of the features underground (Fig. 6,7,8C) and contain primary carbonate minerals which are predominantly dolomite (some Fe-bearing) and lesser calcite. Euhedral dolomite and calcite rhombs up to 3 cm in size are intergrown with sulphide and magnetite (Fig. 13F,G), with no systematic variation or zonation across and within the veins/patches, including the margins. Carbonate crystals often host sulphide inclusions which are present as fractionated blebs comprising pyrrhotite, pentlandite, chalcopyrite, magnetite and minor pyrite (Fig. 13G).

7.3 Disseminated interstitial sulfides in ultramafic and poikilitic gabbro rocks

Some of the ultramafic rocks contain coarse interstitial blebs and aggregates of sulfide (Fig. 12E,F). Clearly these were present as crystallised phases in the ultramafics prior to brecciation and injection of the massive sulfides. The aggregates comprise of pyrrhotite-pentlandite-chalcopyrite alongside magnetite, ilmenite and minor pyrite and apatite (Fig. 12E,F). Some of the poikilitic gabbros also contain minor interstitial blebs of pyrrhotite-pentlandite-chalcopyrite assemblage (Fig 13H).

8. U-Pb geochronology

Zircons were extracted from two samples of Munali igneous rocks from drillhole MAD036: a poikilitic gabbro (from a depth of 155 m); and an ultramafic phoscorite pegmatite (from a depth of 216 m). The mineralogy and texture of the samples are shown in Figure 14A-D, and typical textural association of zircons are shown in Figure 14C and D. The results are shown as conchordia plots in Figure 14 E and F, and the full data is presented in Table 2.

The sample of poikilitic gabbro returned a CA-TIMS age of 862.39 ± 0.84 Ma, based on a $^{206}Pb/^{238}U$ weighted average from four concordant and overlapping zircons (Fig. 14E, Table 2). This is within the error of the 852 ± 22 Ma for a sample of pegmatitic gabbro from the CGU that is cited in Johnson et al. (2007), but provides a much more precise age. One other zircon in the separate gave an age of 865.63 ± 2.26 Ma (Table 2; Fig. 14E), which was not included in the weighted average for the interpreted age and is considered to be inherited, possibly from the main CGU.

The zircons in the ultramafic sample from the MUBU produced a U-Pb age of 857.9 ± 2.1 Ma, based on a $^{206}Pb/^{238}U$ weighted average from four concordant and overlapping zircons (Fig. 14F, Table 2). This is marginally, but distinctly younger (by at least 1.55 Ma allowing for the 2σ errors) than the gabbro, and confirms the geological relationships that indicate the ultramafics intruded the gabbro. An interesting feature about the zircons from this rock is the very high model Th/U of 14-22 (Table 2), compared with 0.6-0.9 in the gabbro. This appears to be due to the very low U content of the zircons in the ultramafic (3-10 ppm). This distinct geochemical characteristic between the two samples illustrates that these are two distinct populations, and the ultramafic zircons are not inherited xenocrysts from the gabbro.

9. Discussion

Our detailed field data and supporting geochronology and petrological work allows a number of advances to be made in our understanding of the Munali deposit, but also poses a number of questions relating to:

1. The relative and absolute timings of events in a multi-stage magmatic, mineralisation and tectonic history;
2. The possible sources of magma for the multiple stages of magmatism, especially for the phoscorites, and their relation to sulfide mineralisation;
3. The physical mechanisms of sulfide emplacement, brecciation and deformation;
4. The unusual association of a magmatic sulfide assemblage of pyrrhotite-pentlandite-chalcopyrite(-magnetite) with abundant carbonate and apatite.

We explore each of these aspects below and provide a number of constraints on any genetic models developed for the Munali intrusion and mineralisation.

9.1 Timing of multi-stage magmatic emplacement

We interpret that the intrusion of the CGU is the first stage in the development of the MIC. The Complex is lozenge shaped at outcrop and appears to be conformable within the main marble unit of the Lower Nega Formation in the area. The variable texture, from microgabbro, through medium- to coarse-grained gabbro may suggest multiple stages of intrusion but we suggest that all gabbroic rocks are likely to be cogenetic. The field relations and drill core information clearly indicate emplacement of the gabbro preferentially and conformably into the marble unit, and that the intrusion created space, and most likely assimilated some of the host rock given the carbonate-rich ‘hybrid’ zone at the hangingwall contact (Fig. 2, 4C). The poikilitic gabbro is present within the MUBU, and may have been a marginal unit prior to intrusion of the ultramafic rocks as it is present in some of the hybrid zones adjacent to the marble contact, though similar rocks with trachytoidal textures are present within the main body of the CGU as well. The poikilitic gabbro is comparable to the gabbros of the CGU in mineralogical composition and only the texture is distinct. Our precise U-Pb date of 862.39 ± 0.84 Ma for the poikilitic gabbro is within the error of the U-Pb SHRIMP zircon CGU date of 852 ± 22 Ma from Johnson et al. (2007), and we suggest that both the CGU and the poikilitic gabbro are related and most likely coeval, and were emplaced closer to our CA-TIMS date of 862 Ma as part of the same magmatic event. The one outlying zircon in the poikilitic gabbro dataset with a date of 865.63 ± 2.26 Ma may represent an inherited crystal from the main CGU. Nevertheless, we consider the mafic rocks to have formed through the same event from a common source.

The ultramafic rocks postdate the CGU on geological grounds (Fig. 10B,C). Evidence for ultramafic rocks crystallised in situ within the MUBU is rare, but is observed in places where some of the pegmatitic portions clearly intrude the footwall gabbro (Fig. 9B,C). Our ultramafic age comes from one such intrusion, placing emplacement of the ultramafic, sulfide-magnetite-apatite-bearing rocks at 857.9 ± 2.1 Ma, some ~4 Ma after the emplacement of the gabbroic rocks. The clear majority of ultramafic rocks in this unit are present as blocks within the sulfide megabreccia, and thus our date provides a maximum age for the deposit, given that the ultramafic rocks are subsequently brecciated by sulfide.

The brecciation also means it is difficult to ascertain whether the ultramafic clasts were brecciated *in situ* (and as such, were emplaced along the margins of the gabbro prior to brecciation and the main period of sulfide emplacement); or they are autoliths or xenoliths of ultramafic rocks transported from a magma chamber elsewhere in the system, and entrained along with the sulfides; or that both these processes occurred. The very large grain size, cumulate texture and the whole, rather than skeletal, nature of the olivines are indicative of slow growth may be more consistent with formation in a larger chamber elsewhere. As such, much of the ultramafic material in the MUBU may have been emplaced as autoliths formed up or down dip of their current position. An insight may be gained by considering the contrast in textures between the coarse-grained olivinite and allied rocks, and the thin olivine basalt dykes, which seem to have been emplaced in-situ but before the end of the sulphide brecciation episode. These latter contain small, skeletal (hopper) olivine phenocrysts and fine-grained scalloped-margin plagioclase laths with high aspect ratios, which suggests they were emplaced with a certain degree of undercooling, possibly at shallow depths.

The fact that many of the ultramafic rocks have interstitial magnetite-sulfide-apatite-(and the zircons we dated) assemblages (Fig. 12E,D) indicates crystallisation with immiscible sulfide liquid (and possibly an Fe-Ti-P liquid as well), prior to brecciation by the main sulfide liquids that form the matrix to the megabreccias. Alternatively, the textures seen in Figures 12 E and D could be interpreted to represent sulfide being injected along olivine grain boundaries during transport/breccia emplacement. This may suggest that the ultramafic cumulates were a partly consolidated ad- or mesocumulate, whose residual interstitial liquid has been displaced by the liquid sulfide.

The definition of a clear emplacement age for the ultramafic allows us to interpret the intrusion mechanism and orientation of the MIC. Although younger than the gabbroic rocks, the 4 Ma gap between the intrusion of the ultrmafics makes it unlikely that they were intruded into significantly different tectono-sedimentary settings. Rifting of the Zambezi basin is bracketed by the Kafue Rhyolite Formation, deposited at 880 Ma, and by the intrusion of the Lusaka and Ngoma granitoids at 820 Ma (Johnson et al., 2007). An emplacement age of ~860 Ma would most likely place its intrusion during this rifting and basin development, and Evans (2011) suggested that this was most likely at a relatively high level into platform sediments. This constraint therefore implies emplacement as a relatively horizontal sheet or sill for both the CGU and the ultramafics. However, it is important to note that the ultramafic age gives a maximum age for the main sulfide mineralisation event as sulfides are clearly injected as the breccia matrix to clasts of ultramafics.

Whilst Figure 11B-C illustrates potentially open parts of the MUBU at depth, it is worth stating that these need not necessarily taper into flute-shaped feeders. They may be part of an anastomosing network of MUBU rocks emplaced along the margin of the CGU, and as such, each possible ‘feeder’ shown on Figure 11 may expand out and reconnect with others. The variability in the thickness of the MUBU both along strike, and with depth in the mined section (from <10 m at surface at Enterprise to ~ 40 m at the deepest section of the mine) shows that a pinching and swelling of the MUBU is present, and potentially controlled by larger structural zones (as seen by the ‘gaps’ in MUBU distribution along strike Figure 11). The geochronological constraints would imply that both units were emplaced as subhorizontal intrusions, meaning the morphology of the MUBU as represented in Figure 11 could be interpreted as anastomosing, horizontal channel-like structures, rather than subvertical feeders.

The final magmatic stage is the intrusion of the olivine dolerite dykes that appear to preferentially intrude the marginal zone, but are then subsequently brecciated by the sulfides.

The degree of brecciation is relatively minor and we interpret this as being a result of intrusion in the latter stages of brecciation, after the main emplacement of sulfide, but prior to the final sulfide remobilisation or injection events. Given that these dykes post-date the ultramafic rocks on these geological grounds, they are younger than 858 Ma.

9.2 Sources of magmas

A detailed geochemical and isotopic assessment of the igneous rocks will be presented elsewhere, but at this stage we can suggest some possibilities for the distinct magmatic phases based on the tectono-chronological setting. The ages of the CGU, poikilitic gabbro and ultramafics are consistent with an emplacement during rifting of the Zambezi basin during the breakup of Rodinia. It is unclear whether the Zambezi Ocean ever developed any true oceanic crust, though John et al. (2003) interpret eclogites in the Zambezi belt, just to the north of Kafue (Fig. 1) to represent Neoproterozoic oceanic crust. Whilst the CGU at Munali is clearly an intrusive body, the timing of its emplacement would make a within plate source a possibility. The clear temporal distinction between the mafic and ultramafic rocks, and the more unusual composition of the latter, indicates that the MIC is not simply a differentiated body of ultramafic-mafic magma, and may represent the result of focussing of more than one magma along the same conduit.

The presence of sulfide breccias hosted by ultramafic rocks is a common feature in many Ni sulfide deposits, but possibly the most significant aspect about Munali in terms of its genesis, is the nature of those ultramafic rocks. The ultramafics are very coarse olivine cumulates with abundant magnetite and some apatite, but no chromite or appreciable pyroxene. There is no IUGS classification name for a rock made entirely of olivine and magnetite, however, the presence of apatite allows their classification as phoscorites (c.f. pyroxenites, chromitites and dunites in more conventional deposits). Phoscorites characteristically contain very low Cr (Krasnova et al., 2004), which would explain the absence of any chromite in the Munali system, and olivines with high forsterite content, consistent with those we present in Table 1. Phoscorites are almost always related to carbonatites (Krasnova et al., 2004), which are commonly associated with rifting in intraplate settings. This is consistent with a syn-rift emplacement age for the phoscorites of 858 Ma but would require a deep mantle source as they are considered to be primary mantle melts (Jones et al., 2013). We note that the Munali ultramafics are not nelsonites (apatite-magnetite or apatite-magnetite-gabbronorite rocks) commonly associated with anorthosite massifs (e.g. Dymek and Owens, 2001).

Whilst the abundant carbonate content of the Munali ores is likely to be at least in part due to assimilation of carbonate wall rocks, the phoscorites (and by extension, carbonatites) raise the possibility that some, if not the majority of the carbonate may be of a primary magmatic source. Carbonatite intrusions are present sporadically throughout the Zambezi belt into Mozambique (Walsh et al., 2001), and form a linear trend that runs ESE from the Munali area across the border into northern Zimbabwe. Just 35 km to the east of Munali, at Kesya, there is an irregular carbonatite breccia body of unknown age that has been interpreted as being formed through fluidised systems, with gas streaming through networks of channels carrying xenoliths and carbonate crystals (Smith, 1963). There are some parallels to be drawn with the 'fluidised' textures in the Munali ore breccia (Fig. 8H). Across the border into Zimbabwe lie several carbonatites at Marindagomo, Dande-Doma and Kapfrugwe which all contain apatite and magnetite with carbonate according to the brief descriptions in Walsh et al. (2001). None of these intrusions have been dated although they have been deformed at around 800 Ma (Walsh et al., 2001) and so it is quite possible that the 858 Ma phoscorite event may be related to these carbonatite intrusions, and that intra-plate rifting at the time was associated with carbonatitic as well as mafic magmatism.

9.3 Brecciation and sulfide emplacement

Clearly the MUBU has undergone a complex multi-stage history of multiple magma injections, brecciation, deformation, faulting, sulfide injection and hydrothermal alteration/metasomatism. Unravelling these events has been extremely challenging, especially in the early exploration days where only drillcore was available. Now, with our underground mapping, we can define a distinct geological framework to explain some of the complex features of the orebody.

Brecciation is present on every scale (Fig. 6,7,8 and Fig 13A) and a key distinction in determining a geological model for the deposit is whether the brecciation event is a primary magmatic event, with igneous clasts transported (and brecciated) in a matrix of sulfide liquid and silicate melt(s), or whether it is a tectonic breccia, with sulfide introduced or remobilised during deformation and metamorphism. Our geochronological and geological framework allows us to place some constraints on this. The poikilitic gabbro and the ultramafic rocks are brecciated and infilled by sulfide. As such, brecciation must have occurred after the ultramafic emplacement age of 858 Ma, though it may quite likely be part of the same magmatic event.

Towards the footwall contact there is clear evidence of the presence of sulfide liquids that injected the footwall, and also infilled the matrix to breccias on multiple scales. The decrease in clast volume in the sulfide matrix portion (and subsequent increase in sulfide proportion of the matrix) towards the footwall contact is consistent with gravity sorting of a dense sulfide liquid-silicate clast slurry, with the densest material being concentrated at the base, forming the most massive sulfide concentrations at the footwall contact. This is likely to have formed from a matrix melt network of sulfide and silicate liquids, with clasts of ultramafics and poikilitic gabbro. Whilst many magmatic breccias contain both autoliths of igneous rocks and country rock xenoliths (e.g. Voisey's Bay, Canada; Li and Naldrett, 1999), there are no recognisable metasedimentary rock xenoliths at Munali. The hybridised nature of the hangingwall contact (Fig. 4C) is compelling evidence for the interaction at high temperatures between silicate magma and the marble host rock, and that the magma fully assimilated any metasedimentary xenoliths. The Munali breccia can be considered to be primarily a magmatic breccia, with sulfide liquid present within a matrix of silicate melt and pre-formed igneous clasts.

The penetration of sulfide into the footwall gabbro (Figs. 7,8) shows evidence for at least some downward propagation of sulfide; a feature also documented by Samur et al. (2015) at Voisey's Bay. Furthermore, the penetration and subsequent brecciation of the footwall gabbro appear to show analogous textures to those that Barnes et al. (2016) show for the Oktyabrsky Mine, Talnakh, Siberia and Dowling et al. (2004) show at the Silver Swan komatiite-hosted deposit, Western Australia, whereby sulfide liquids have melted, and 'floated off' rafts of footwall rocks. On a smaller scale, Figure 13A shows angular clasts on a centimetre scale remarkably like that shown on a metre scale in Figures 7 and 8. This brecciation of the silicate clasts is likely to have formed from disaggregation by infiltration of sulfide liquids along cracks and grain boundaries, and this has been shown to occur in the massive sulfide ores at Kambalda (Seat et al., 2004). This key observation implies that sulfide liquid was present not only during brecciation but that sulfide liquids may also have induced fracturing, particularly in zones where massive sulfides are present. The penetration into the footwall and 'floating off' of xenoliths is also compelling evidence that the footwall contact was the true base of the MUBU during emplacement.

Further evidence for the presence of liquid sulfide lies in the common magnetite reaction rinds present at many massive sulfide-silicate rock boundaries, including at the footwall contact (Fig. 8A) and around the margins of sulfide-enclosed xenoliths in the breccia (Fig. 8E). Rinds of oxide at sulfide-silicate boundaries have been identified in many komatiite-hosted sulfide deposits (Groves et al., 1977; Frost and Groves, 1989; Barnes et al., 2016; Staude et al., 2016), although in these cases the oxide is normally chromite, formed due to disequilibrium at what is interpreted to be the interface between sulfide liquid and komatiitic silicate melt. The Munali system is very Cr-poor, and so in the absence of significant Cr in the silicate rocks, any such reaction is likely to form magnetite. If analogous, we interpret the common magnetite rinds at the boundary between sulfide and silicate rocks to have formed from melt interaction between sulfide liquid and a silicate melt film generated by melting of the silicates by the molten sulfide liquid; or alternatively as a solid state disequilibrium reaction.

Whilst the massive and semi massive sulfides can be relatively simply explained by the presence of sulfide liquid within the matrix of a magmatic breccia, the later stage carbonate-magnetite-sulfide veins and intrusions are more unusual. These are the latest stage of sulfide-bearing veins/injections we have identified, but are comprised of an apparently high-temperature, primary assemblage of dolomite/calcite, magmatic sulfides and magnetite. The presence of fractionated inclusions of subrounded sulfide within carbonate crystals (Fig. 13G) implies trapping of solidified sulfide blebs. The lack of negative crystal shapes would suggest that the sulfide was not trapped as a liquid by the dolomite/calcite; though the temperature of crystallisation of the carbonate phase is unclear. There is no systematic variation or zonation across and within the veins/patches, including the margins, which would be indicative of crystallisation from a fluid phase, and so we interpret these to be magmatic, high temperature veins.

The carbonate could represent the product of an extremely fractionated, late stage carbonate-rich melt with carbonate sourced from contamination from the country rocks. However, there are many Ni sulfide deposits around the world are intruded into carbonate rocks (e.g. Jinchuan, Noril'sk), and whilst they do show carbonate veins, they do not show many of the unusual features that Munali does, none more so than the phoscorite association, which may support an alternative source for the carbonate. Given the presence of atypical ultramafics at Munali and the phoscorite-carbonatite association mentioned above, the carbonate in these late stage veins may represent a carbonatite melt but whether the sulfide was transported within such a melt, or was remelted by it is, as yet, unclear.

Magmatic emplacement and brecciation at Munali was a multi-stage process, and, as stated above, the olivine basalt/dolerite dykes appear to have been intruded into the MUBU after initial sulfide emplacement, but have subsequently been subject to disruption and brecciation and further sulfide injection, including the late-stage carbonate-magnetite-sulfide veins. Considering that the MIC has undergone deformation and metamorphism during the Pan African/Lufilian orogeny then it is worth considering the possibility that at least some of the sulfide injections may have occurred during deformation, as solid-state injections. This is the case for the Selebi-Phikwe magmatic sulfide deposits in eastern Botswana (Maier et al., 2007). In deposits that have undergone metamorphism and tectonism, such as at Selebi-

Phikwe, durchbewegung textures (Marshall and Gilligan 1989) can be a characteristic feature of the semi-massive ores. In such cases, these are manifest as a strongly foliated matrix with rounded clasts of more competent silicate material that have been plucked or separated from their source, kneaded and milled with a sense of rotational movement, which occurs in the solid state. This is clearly shown in Figure 2e,f of Maier at al. (2007) at Selebi-Phikwe. However, in comparison, the Munali sulfide breccias display an abundance of much more angular clasts (Fig. 12A), and whilst rounded clasts do exist (Fig. 12D), the clast population is dominated by angular clasts on millimetre (Fig. 12D), centimetre (Fig, 12A) and metre (Fig. 6, 8E) scales, and the matrix is not strongly foliated. We consider that any solid state remobilisation that may have occurred at Munali is minor, localised and secondary, and that the evidence we present is strongly consistent with at least initial brecciation and emplacement of sulfide liquids at high temperature as part of a dynamic magmatic system.

Notwithstanding this, there is evidence of tectonic deformation within the Munali breccia unit is the form of the sheared, ductile fabrics exhibited by many of the talc-carbonate altered clasts (Fig. 9A,H). Their presence, in zones adjacent to relatively unaltered ultramafics implies heterogeneous alteration within the orebody and the possible presence of discrete fluid pathways, or juxtaposition during brecciation. Alteration of ultramafic rocks to serpentinite can progress to an assemblage of talc and magnesite through the interaction of a CO_2-bearing fluid with serpentine and is common in many ultramafic rocks (e.g. Donaldson, 1981; Barnes et al., 2009). The talc-carbonate altered clasts at Munali show asymmetric and flattened textures suggestive of ductile deformation and shearing (Fig. 8A, 9A), but do not necessarily form in planar zones. Figure 9H illustrates a good example of the ductile fabrics flowing around a more rigid clast of less altered ultramafic rock. The nature of the breccia means that there are large contrasts in rheology several scales. The softest rock types would be the talc-carbonate altered rocks and the sulfides themselves, and thus the highest strain in any deformation will be manifest in zones that contain an abundance of this rock, if alteration occurred prior to deformation. It is worth noting that the sulfides are only moderately deformed, and usually where they are part of a sheared talc-carbonate dominated zone (e.g. Fig. 9A). At the other end of the scale, the olivine dolerites and gabbros are the most competent, and there is little evidence of any ductile deformation in these rocks. We suggest, therefore, that talc-carbonate alteration of zones of ultramafic clasts occurred after brecciation, resulting from the interaction with CO_2 bearing fluids channelled through parts of the breccia unit, and that these zones preferentially took up strain during later deformation. The source of the CO_2 is likely to be from devolatilisation of the country rock marbles, or any potential carbonatite melt.

9.4 Sulfide mineralogy and constraints on sulfide saturation

The Fe- and Ni-rich and Cu-poor nature of the Munali mineralisation can be explained in two ways. Such an assemblage is typical of very early stage sulfide saturation in a Mg-rich magma prior to extensive fractionation, which removes Ni into olivine and pyroxenes and produces lower Ni/Cu ratios in any subsequent sulfides. Early stage sulfide saturation would be consistent with a contamination-driven model for ore genesis, which, given the evidence for the assimilation of sulfide-bearing marble upon emplacement, is entirely possible. Secondly, it is possible that an originally Ni- and Cu-rich sulfide had fractionated, with the Ni crystallising as mss (this being the portion preserved at the mine) and with the majority of the Cu-rich residual sulfide liquid having migrated away and accumulated elsewhere in the system. The Ni/Cu ratio at Munali of around 10 (CNM, 2016) is at the upper limit of mafic-ultramafic intrusion hosted deposits, with only komatiites hosting sulfides with higher Ni/Cu ratios than 10 (Barnes et al. 2017). Thus, the deposit could simply be a Ni-rich, Cu-poor system, or there is a significant Cu-rich sulfide body elsewhere in the system as is seen at Sudbury, where Cu-rich portions are typically found at depth due to the migration of fractionated Cu-rich sulfide liquid (e.g. Li and Naldrett, 1992). However, an important consideration here is that the sulfide composition appears to be similar over multiple sulfide events (Mitchell 2016), which would be inconsistent with sulfide fractionation, which may be expected to display greater variations in Ni/Cu between each event. Ongoing work on the base and precious metal geochemistry of the sulfides should shed light on this, and will be presented elsewhere.

Although we have identified a number of different textural styles and associations of sulfide mineralisation, the overall composition of the sulfide portion itself similar, even in the carbonate associated assemblage (Fig. 13G). This may indicate that whilst there were multiple injections of sulfide into the MUBU, there may have been a common, homogenous source for these in the system. The breccia fill massive sulfides and the interstitial sulfides in the ultramafics or poikilitic gabbros may be related, though a clear link would require geochemical and isotopic fingerprinting. That said, the presence of sulfides within blocks of ultramafic rocks that have later been brecciated and injected by massive sulfide gives evidence for sulfide saturation during the formation of the ultramafic rocks; but also that these rocks crystallised before being disrupted and entrained in a later sulfide-matrix breccia.

A particularly unusual feature of the associated mineralogy of the sulfides at Munali is the presence of abundant (and often very large) apatite crystals. Apatite is present in some of the more massive sulfide assemblages, but is not ubiquitous, indicating it may be a feature of one particular sulfide injection event. Apatite-oxide assemblages (nelsonites) are typically associated with massif-type anorthosites as nelsonites (e.g. Ashwal 1993) or in segregated layers in various layered intrusions, such as Bushveld, Skaergaard and Stillwater (Hanley et al., 2008; Namur et al., 2012). However, the association of apatite and Fe-Ti oxides with Ni-Cu-Fe-sulphides and mafic silicates seen at Munali is rare. Only two other deposits have similar textures documented: the Babbit deposit of the Duluth Complex, Minnesota (Ripley et al., 1998), and the Itsindro Gabbro Complex, Madagascar (Augé et al., 2015). Both of these deposits also show euhedral apatite crystals hosted within, or in close proximity to, pyrrhotite-pentlandite and magnetite-ilmenite assemblages and interpret the texture to be the result of the presence of immiscible sulfide and Fe-Ti-P liquids. This may be a plausible mechanism for the presence of abundant apatite and magnetite in some of the massive sulfides at Munali, although the source of the Fe-Ti-P liquid, and whether it separated from a more Si-rich liquid (e.g. Veksler 2007) is unclear at present, as is the significance of the abundant carbonate with this process. The large size of many of the apatites (Fig. 13C) may indicate significant volatile activity during their formation. Another explanation may be that they represent disaggregated crystals from phoscorites broken up by the sulfide-induced brecciation as described above. There is supporting evidence for this in the observation that the apatite bearing sulfide assemblages have notably more magnetite as well. An alternative possibility, and one that also goes a way to explaining the carbonate association as well, lies in the similarity between the sulfide-apatite-carboante textures seen in the ores at Munali and recently recognised sulfide-apatite-carbonate assemblages in melt veins in mantle xenoliths, interpreted to represent sulphide-carbonate-phosphate immiscibility (Hughes et al., 2016). If they are comparable, the origin of the apatite may be primary magmatic melts, related to the apparently magmatic carbonate, and would provide a stronger case for a carbonatite influence at Munali.

9.5 Developing an emplacement model for Munali

The regional Neoproterozic geological framework for the Munali area is summarized in Figure 15. The magmatic and mineralisation events at Munali clearly fit into the regional basin development of the Zambezi proto-ocean, though the deformation present in the MUBU could be related to the later Pan African (Lufilian) event around 550-520 Ma. No dates for the chain of carbonatites into northern Zimbabwe are known, though they are thought to have been deformed around 800 Ma, which coincides with the granitic magmatism interpreted by Johnson et al. (2007) to represent the end of basin development.

For the MIC in detail, based on the key field relationships and geochronological data we have presented the following sequence of events can be defined:

- Emplacement of the CGU, with poikilitic gabbro into marbles of the Nega Formation as a sill at 862 Ma.

- Crystallisation of ultramafic rocks with interstitial sulfides at 858 Ma
- Formation the MUBU by the injection of silicate magma with autoliths/xenoliths of ultramafics and poikilitic gabbro, and sulfide liquid; accompanied by major brecciation driven by the injection of dense sulfide liquids
- Intrusion of olivine basalt/dolerite into the MUBU
- Interaction of a carbonate-rich phase, altering ultramafic clasts to talc-carbonate and possibly also injecting the carbonate-magnetite-sulfide veins
- Further brecciation and focussed ductile deformation of talc-carbonate altered rocks

Whilst this work has developed a clear geological framework in terms of the timing of events, there are a number of key features that require further investigation in order to test aspects of the model presented here, including (1) classifying the geochemistry and origin of the igneous phases, (2) determining the triggers for S saturation and the role of crustal contamination, (3) unravelling the volatile story and carbonate sources and the timing of talc-carbonate alteration and any effect on sulfide mineralogy, (4) the origin of the abundant apatite, (5) a full investigation of the sulfide geochemistry, mineralogy and tenors, and (6) developing an integrated model for the dynamic environment of emplacement and reworking.

9.6 Implications for models of Ni sulfide ore genesis

In terms of setting, Munali is classically located near to a craton margin and intruded during intraplate rifting, as many of the world's significant Ni deposits are (Begg et al., 2010). However, the unusual characteristics of the associated igneous rocks at Munali potentially indicate an otherwise rare, or poorly constrained, association with phoscorite-carbonatite intrusions. This, and a number of other lines of evidence (high temperature carbonate, apatite-magnetite-carbonate assemblages, CO_2 fluid activity) point strongly towards a carbonatite influence on the magmatism at Munali. Whilst sulfides have been recorded in phoscorites, e.g. Kovdor, Kola Peninsula, Russia (Krasnova et al., 2004) and PGE are recovered as a significant by-product at Phalaborwa, South Africa, Munali is by far the most significant Ni deposit associated with such rocks, and the only one thus far recognised to have a possible sulfide-bearing carbonatite melt as an integral part of the orebody. Phoscorite intrusions are very rare worldwide, but Munali shows that magmatic sulfide mineralisation can form in such systems, and produce economic concentrations of Ni-Cu-PGE sulfides. At this stage, the sources of magma are unclear, but the critical control of deep seated fault systems allow for the passage of magmas potentially from different sources. Munali seems to demonstrate that both mafic magmatic systems, and more exotic phoscoritic-carbonatitic melts may use the same crustal pathways and potentially interact to form Ni-Cu-PGE deposits.

The micro and macrotextures of the orebody itself, including the brecciation by sulfide liquids, reaction rinds of magnetite formed by sulfide-silicate melt interaction, and ductile deformation of talc-carbonate altered zones represents an opportunity to distinguish the physical mechanisms of magmatic versus tectonic deformation. Our observations show that sulfide liquids have been fundamental, at least towards the base of the orebody, in driving the physical processes of brecciation. Furthermore, the clear downward movement of large volumes of sulfide liquids in conduit systems has implications for the major process of ore genesis: that of sulfide saturation. The downward flow through a sub-vertical conduit, or lateral flow along sub-horizontal sheet-like portions of magmatic plumbing systems means that sulfide saturation may have occurred at a level above the current position of the orebody; which is most likely now eroded away. Hughes et al. (2016) demonstrate this for ultramafic plugs in Rum, Scotland, where the S isotope ratios of the sulfides in the plugs could only have been acquired from Jurassic sediments present at levels above the current erosion level. Conversely, in some deposits, there is clear evidence from multiple S isotope studies that sulfides have been transported upwards through conduit systems (e.g. the Platreef, South Africa; Sharman et al., 2013; Eagle deposit; Ding et al., 2011), though in the case of the Platreef at least, this relates to the transport of small droplets, rather than voluminous slurries of sulfide. This illustrates that S isotope studies of rocks not just below and in contact with mineralised magmatic conduits, but also present above them, must be assessed and may provide evidence for upward versus downward sulfide movement; critical to accurate models of ore genesis.

10 Summary

The Munali Ni sulfide deposit conforms to many of the classic features of magmatic sulfide deposits formed in conduit systems: location close to a craton margin, timing coincident with intraplate-rifting, emplacement as a dyke-sill complex along a major crustal lineament, crystallisation as a mafic-ultramafic intrusion with a chonolith-like morphology, and mineralisation present as massive and semi-massive sulfide in a magmatic breccia. However, the deposit shows a highly complex and unusual multi-stage history that shows a clear temporal distinction between an early mafic phase, and a later, mineralised ultramafic intrusion. Further atypical features of the Munali deposit are the strong apatite-magnetite-carbonate character of the orebody and the composition of the ultramafics as phoscoritic. These two aspects may be related and Munali could represent an example of a magmatic Ni sulfide deposit with a significant phoscorite-carbonatite influence.

11 Acknowledgments

The management of Consolidated Nickel Mines, especially Simon Purkiss, are thanked for their assistance with setting up the fieldwork, providing a research funding for this project, including the MGeol projects of CLM, GAH and LAW; and for granting permission to publish. The staff of Mabiza Resources at the Munali Nickel Mine, including Danny Musemeka, Peter Munkondya, and Matt Banda, are thanked for logistical support on site in Zambia and for facilitating underground work. Reviews by Steve Beresford and John Hronsky are acknowledged for providing positive and helpful suggestions in improving the manuscript. The geochronology was funded by a Society of Economic Geologists Student Research Grant awarded to GAH. Discussions in the field with Darryl Mapleson, Daryl Blanks and Rob Moore are acknowledged. Clare Kelly is thanked for technical support with Micromine and Shaun Graham for assistance with Mineralogic mapping at Zeiss and support for LAW's MGeol project.

REFERENCES

Albidon. 2006b. Positive bankable feasibility study for enterprise nickel deposit at Munali Project, Zambia. News release 17 August 2006.

Ashwal, L., .D., 1993, Anorthosites. Berlin, Heidelberg, New York, Springer-Verlag, 422 p.

Augé, T., Bailly, L., and Roig, J.-Y., Evidence for Fe-Sulfide and Fe-Ti Oxide Liquid Immiscibility in the Itsindro Gabbro Complex, Madagascar in André-Mayer, A. S., Cathelineau, M., Muchez, P., Pirard, E., and Sindern, S., 2015, eds., Mineral resources in a sustainable world, Proceedings of the 13th Biennial SGA Meeting, Nancy, France, 2134 p.

Barnes, S.J., Wells, M.A. and Verrall, M. R., 2009, Effects of Magmatic Processes, Serpentinization, and Talc-Carbonate Alteration on Sulfide Mineralogy and Ore Textures in the Black Swan Disseminated Nickel Sulfide Deposit, Yilgarn Craton, Economic Geology, 104, 539–562.

Barnes, S. J., Cruden, A. R., Arndt, N. T., Saumur, B. M., 2016, The mineral system approach applied to magmatic Ni-Cu-PGE sulphide deposits, Ore Geology Reviews, v. 76, p. 296-316

Barnes, S. J., Beresford, S. W. and Le Vaillant, M., 2016, Interspinifex Ni sulfide ore from the Coronet Shoot, Kambalda: characterization using microbeam X-ray fluorescence mapping and 3D X-ray Computed Tomography, Economic Geology, 111, 1509-1517.

Barnes, S.J., Holwell, D.A., Le Vaillant, M, 2017, Magmatic sulfide ore deposits. Elements

Begg, G. C., Hronsky, J. A. M., Arndt, N. T., Griffin, W. L., O'Reilly, S. Y., and Hayward, N., 2010, Lithospheric, Cratonic, and Geodynamic Setting of Ni-Cu-PGE Sulfide Deposits, Economic Geology, v. 105, p. 1057–1070, doi:10.2113/econgeo.105.6.1057.

Bingen, B., Jacobs, J., Viola, G., Henderson, I.H.C., Skår, Ø., Boyd, R., Thomas, R.J., Solli, A., Key, R.M., and Daudi, E.X.F., 2009, Geochronology of the Precambrian crust in the Mozambique Belt in NE Mozambique, and implications for Gondwana assembly. Precambrian Research, 170, 231-255.

CNM, 2016, The Munali Nickel Mine: Offering Near-Term Brownfields Production in Zambia, Factsheet, 2 pp

Donaldson, M. J., 1981, Redistribution of ore elements during serpentinization and talc-carboante alteration of some Archaen dunites, Western Australia, Economic Geology, 76, 1698-1713.

Dowling, S.E., Barnes, Stephen J., Hill, R.E.T., Hicks, J., 2004. Komatiites and nickel sulfide ores of the Black Swan area, Yilgarn Craton, Western Australia, 2. Geology and genesis of the orebodies. Mineralium Deposita 39, 707–728

Ding, X., Ripley, E.M., Shirley, S.B., Li, C., Moore, C.H., 2011, Os, Nd, O and S isotope constraints on the importance of country rock contamination in the generation of the conduit-related Eagle Cu-Ni-(PGE) deposit in the Midcontinental Rift System, Upper Michigan: Geochimica et Cosmochimica Acta, 89, 10-30

Dymek, R.F., Owens, B.E., 2001, Petrogenesis of Apatite-Rich Rocks (Nelsonites and Oxide-Apatite Gabbronorites) Associated with Massif Anorthosites. Economic Geology, 96, 797–815

Evans, D.M., 2005, Geology and geochemistry of the Munali Nickel Deposit, Consulting Report, Carrog Consulting, 34 p.

Evans, D. M., 2011, Geodynamic setting of Neoproterozoic nickel sulphide deposits in eastern Africa, Applied Earth Science (Trans. Inst. Min. Metall. B), v. 120 (4), p. 175-186.

Fleet, M.E., Chryssoulis, S.L., Stone, W.E., and Weisener, C.G., 1993, Partitioning of platinum-group elements and Au in the Fe–Ni–Cu–S system: experiments on the fractional crystallization of sulfide melt. Contributions to Mineralogy and Petrology, 115, 36–44.

Frost, K.M., and Groves, D.I., 1989, Magmatic contacts between immiscible sulfide and komatiitic melts; implications for genesis of Kambalda sulfide ores: Economic Geology, v. 84, p. 1697–1704

Goscombe, B., Armstrong, R., and Barton, J.M., 2000, Geology of the Chewore Inliers, Zimbabwe: Constraining the Mesoproterozoic to Palaeozoic evolution of the Zambezi Belt: Journal of African Earth Sciences, v. 30, p. 589–627.

Groves, D.I., Barrett, F.M., Binns, R.A., and McQueen, K.G., 1977, Spinel phases associated with metamorphosed volcanic-type iron-nickel sulfide ores from Western Australia: Economic Geology, v. 72, p. 1224–1244

Hanley, J. J., Mungall, J. E., Pettke, T., Spooner, E. T. C., and Bray, C. J., 2008, Fluid and Halide Melt Inclusions of Magmatic Origin in the Ultramafic and Lower Banded Series, Stillwater Complex, Montana, USA, Journal of Petrology, v. 39 (6), p. 1133-1160.

Hanson, R. E.; Wilson, T. J.; and Wardlaw, M. S. 1988. Deformed batholiths in the Pan-African Zambezi belt, Zambia: age and implications for regional Proterozoic tectonics. Geology 16:1134–1137

Hanson, R.E., Wilson, T.J., and Munyanyiwa, H., 1994, Geologic evolution of the Neoproterozoic Zambezi orogenic belt in Zambia: Journal of African Earth Sciences, 18, 135–150

Holwell, DA, Keays, RR, Firth EA and Findlay, J. 2014. Geochemistry and mineralogy of platinum-group element mineralisation in the River Valley intrusion, Ontario, Canada: a model for early stage S saturation and multi stage emplacement and the implications for ‘contact-type’ Ni-Cu-PGE mineralisation. Economic Geology, 109, 689-712

Hughes, H. S. R., McDonald, I., Boyce, A. J., Holwell, D. A., and Kerr, A. C., 2016, Sulphide Sinking in Magma Conduits: Evidence from Mafic–Ultramafic Plugs on Rum and the Wider North Atlantic Igneous Province, Journal of Petrology, v. 57, p. 383-416

Hughes, HSR, McDonald, I, Loocke, M, Butler, IB, Upton, BGJ, Faithfull, JW, 2016, Paradoxical co-existing base metal sulphides in the mantle: the multi-event record preserved in Loch Roag peridotite xenoliths, North Atlantic Craton. Lithos. doi:/10.1016/j.lithos.2016.09.035

John, T., Schenk, V., Haase, K., Schere, E.E., and Tembo, F., 2003. Evidence fro a Neoproterozoic ocean in south central Africa from MORB-type geochemical signatures and P-T estimates from Zambian eclogites, Geology, 31, 234-236.

Johnson, S. P., Rivers, T. and De Waele, B. 2005. A review of the Mesoproterozoic to early Palaeozoic magmatic and tectonothermal history of south-central Africa: implications for Rodinia and Gondwana, Journal of the Geological Society of London, 162, 433–450

Johnson, S. P., De Waele, B., Evans, D., Banda, W., Tembo, F., Milton, J. A., and Tani, K., 2007, Geochronology of the Zambezi Supracrustal Sequence, Southern Zambia: A Record of Neoproterozoic Divergent Processes along the Southern Margin of the Congo Craton, The Journal of Geology, v.115, p. 355–374.

Jones, A.P., Genge, M., Carmody, L., 2013, Carbonate melts and carbonatites. Reviews in Mineralogy & Geochemistry, 75, 289-322

Katongo, C., Kolker, F., Klotzli, U., Koeberl, C., Tembo, F., and De Waele, B., 2004, Petrography, geochemistry and geochronology of granitoid rocks in the Neoproterozoic-Paleozoic Lufilian-Zambezi belt, Zambia: implications for tectonic setting and regional correlation, Journal of African Earth Sciences, v. 40, p. 219–244.

Krasnova N. I., Petrov, T. G., Balaganskaya, E.G., Garcia, D., Moutte, J., Zaitsev, A.N., Wall, F., 2004. Introduction to phoscorites: occurrence, composition, nomenclature and petrogenesis. In Phoscorites and Carbonatites from Mantle to Mine: the Key Example of the Kola Alkaline Province, eds. Wall, F and Zaitsev, A. N.: Mineralogical Society of Great Britain and Ireland, London.

Li, C., Naldrett, A.J., 1992, Platinum, palladium, gold, copper-rich stringers at the Strathcona Mine, Sudbury; their enrichment by fractionation of a sulfide liquid. Economic Geology, 87, 1584-1598.

Li, C., Naldrett, A.J., 1999, Geology and petrology of the Voisey's Bay intrusion: reaction of olivine with sulfide and silicate liquids. Lithos, 47, 1-31

Lightfoot, P.C., Farrow, C.E.G., 2002. Geology, geochemistry, and mineralogy of the Worthington offset dike: a genetic model for offset dike mineralization in the Sudbury Igneous Complex. Economic Geology. 97, 1419–1446

Maier, W.D., Barnes, S-J. and Ripley, E.M., 2011, The Kabanga Ni sulfide deposits, Tanzania: a review of ore-forming processes. Reviews in Economic Geology, 17, 217-234.

Maier, W. J., and Groves, D. I., 2011, Temporal and spatial controls on the formation of magmatic PGE and Ni–Cu deposits, Mineralium Deposita, v. 46, p. 841–857.

Maier W. D., Barnes, S.-J., Chinyepi, G., Barton Jr, J.M., Eglington, B., and Setshedi, I., 2007, The composition of magmatic Ni–Cu–(PGE) sulfide deposits in the Tati and Selebi-Phikwe belts of eastern Botswana. Mineralium Deposita, 43:37–60.

Marshall, B., and Gilligan, L.B., 1989, Durchbewegung structure, piercement cusps and piercement veins in massive sulfide deposits: formation and interpretation. Economic Geology, 84, 2311-2319.

McDonald, I., and Holwell, D. A., 2007, Did lower zone magma conduits store PGE-rich sulphides that were later supplied to the Platreef?, S. Afr. J. Geol., v. 110, p. 611–616,

Mitchell, C.L., 2016, Comparison of the style and nature of breccia-hosted Ni-sulphide mineralisation within the Munali intrusion, Zambia, unpublished MGeol thesis, University of Leicester, UK, 80 p.

Naldrett, A.J., 1992, A model for the Ni-Cu-PGE ores of the Noril'sk region and its application to other areas of flood basalt. Economic Geology, 87, 1945-1962

Namur, O., Charlier, B., and Holness, M. B., 2012, Dual origin of Fe–Ti–P gabbros by immiscibility and fractional crystallization of evolved tholeiitic basalts in the Sept Iles layered intrusion, Lithos., v. 154, p. 100-114

Porada, H., and Berhorst, 2000, Towards a new understanding of the Neoproterozoic–Early Palaeozoic Lufilian and Zambezi belts in Zambia and the Democratic Republic of Congo, Journal of African Earth Sciences, v. 30, p. 717–771

Ripley, E. M., Severson, M. J., and Hauck, S. A., 1998, Evidence for sulfide and Fe-Ti-P-rich liquid immiscibility in the Duluth Complex, Minnesota, Economic Geology, v. 93, p. 1052-1062

Ripley, E.M., Lightfoot, P.C., Stifter, E.C., Underwood, B., Taranovic, V., Dunlop, M., Donoghue, K.A., 2015. Heterogeneity of S isotope compositions recorded in the Sudbury Igneous Complex, Canada: significance to formation of Ni–Cu sulfide ores and the host rocks. Econ. Geol. 110, 1125–1135

Seat, Z., Stone, W.E., Mapleson, D.B., Daddow, B.C., 2004, Tenor variation within komatiite-associated nickel sulphide deposits: insights from the Wannaway Deposit, Widgiemooltha Dome, Western Australia. Mineralogy and Petrology, 82, 317–339.

Sharman, E.R., Penniston-Dorland, S.C., Kinnaird, J.A., Nex, P.A.M., Brown, M., Wing, B.A., 2013, Primary origin of marginal Ni-Cu-(PGE) mineralization in layered intrusions: Δ33S evidence from The Platreef, Bushveld, South Africa. Economic Geology, 108, 365-377.

Smith, A. G. 1963, The geology of the country around Mazabuka and Kafue Explanation of degree sheets 1527, SE. Quarter and 1528, SW. Quarter. Rep. 2, Ministry of Labour and Mines, Geological Survey of Northern Rhodesia, 32 pp

Staude, S., Barnes, S.J., Le Vaillant, M., 2016, Evidence of lateral thermomechanical erosion of basalt by Fe-Ni-Cu sulfide melt at Kambalda, Western Australia, Geology, doi:10.1130/G37977.1

Turner, D.C., Rex, D.C., 1991, Volcaniclastic carbonatite at Kaluwe, Zambia: age and relations to sedimentary rocks in the Zambezi rift valley. Journal of the Geological Society, London, 148, 13-15.

Veksler, I.V., Dorfman, A. M., Borisov, A.,Wirth, R., and Dingwell, D. B., 2007, Liquid immiscibility and evolution of basaltic magma, Journal of Petrology, v. 48, p. 2187-2210

Walsh, K.L., Siegfreid, P., Hall, R.P., Hughes, D.J., 2001, Tectonic implications of four recently discovered carbonatites along the Zambezi Escarpment Fault, northern Zimbabwe. Carbonatite Workshop Abstracts, St Etienne, France, 2000, Journal of African Earth Sciences, 32, A36-37.

Figure captions

Fig 1 A: Geological setting of southern Zambia, showing the Zambezi Belt and location of Munali in relation to the Congo and Kalahari cratons at 1Ga (after Evans, 2011); B: location of Munali within the regional setting of the Zambezi Supracrustal Sequence (after Johnson et al. 2007).

Fig 2 Geological map (after Evans, 2005) of the Munali Intrusive Complex showing the major host rock units, and location of the Enterprise, Voyager, Intrepid gossans, the mine portal at the Enterprise mine and drillholes studied and sampled in this work.

Fig 3 A: view looking southeast from the northern part of the Munali Intrusive Complex (gabbro hills), showing the width of the intrusion, the location of the Munali Nickel Mine portal, the Enterprise and Voyager gossans, and the Munali Hills. B: view looking northwest from the Voyager gossan showing the narrowing of the intrusion at the northern end, and the marble outcrop following a topographic valley to the northwest, the Munali Hills to the northeast, and flat arable plains to the southwest. Gossanous outcrops can be seen in the foreground on the left hand side.

Fig 4 Exposures and drill core of rocks within and hosting the Munali Intrusive Complex (MIC). A: outcrop of steeply dipping marble 5 m to the SW of the contact with the MIC at Voyager; B: drill core intersection of marble containing pyrite around 10 m from the contact with the ultramafic unit; C: drillcore intersection (from MAD060) of the hangingwall lithologies and contact with the Munali intrusion along the southwest margin of the intrusion including blebby, carbonate-bearing 'quartzite', biotite-carbonate schist, minor marble, garnet-bearing schists, graphitic schist and the contact marble. Inset shows the diffuse nature of the contact with hybridised ultramafic breccia; D: coarse grained Munali gabbro from the gabbro hills area at the northwest end of the intrusion; E: fine grained dolerite from a dolerite plug in the gabbro hills area; F: gossanous outcrop at Enterprise.

Fig 5 A: plan view of part of the Enterprise underground mine that have been subject to mapping in this study; and B: three dimensional view of the mine workings showing the crosscuts mapped in red.

Fig 6 Underground face maps of cross cuts on the A: 870; B: 845; and C: 820 levels in the Enterprise mine at Munali. View is strike-perpendicular, facing NW, with the gabbro footwall to the right hand side (not exposed in the face as the main drive follows this contact) and the metasedimentary hangingwall to the left hand side; D: example photo-montage of the 820 level. See Figure 5 for location on mine plan.

Fig 7 Underground face maps (A and C) and photo montages (B and D) of the footwall access drives on A,B: the 845; and C,D: the 820 levels, showing the contact relationships between the orebody and the footwall gabbro. View is strike perpendicular, facing NW, with the orebody and main drive on the left hand side. See Figure 5 for location on mine plan.

Fig 8 Underground face maps (A and C) and photo montages (B and D) of the northeastern face of the main drives on A,B: the 845; and C,D: the 820 levels, showing the contact relationships between the orebody and the footwall gabbro. View is strike-parallel. See Figure 5 for location on mine plan.

Fig. 9 Geological features of the Munali orebody exposed in underground faces. A: the footwall contact on the 845 level, with massive sulfide vein marking the base of the mineralised ultramafic unit, sulfide injections into the footwall, and sheared talc-carbonate altered ultramafic clasts indicating downward flow of the sulfide; B: sulfide injections into the gabbro footwall on the 820 level showing variable and non-linear orientations; C: multiple injections of sulfide into the footwall gabbro in the footwall drive of the 870 level showing talc-carbonate-sulfide veins cross cutting massive sulfide veins; D: large clasts of ultramafic surrounded by a matrix of massive sulfide. Much of the olivine-rich ultramafic is serpentinised; E: magnetite reaction rims around clasts of olivine-magnetite ultramafic rock and poikilitic gabbro; F: olivine basalt dyke with minor brecciation infilled with talc-carbonate and sulfide; G: interfingering of ultramafic rocks with olivine dolerite. Serpentine and talc reaction rims form a 2 cm zone at the interface; H: ductile ‘fluidised’ textures of sheared talc-carbonate altered ultramafic clasts within massive sulfide matrix; I: normal fault running strike parallel through the orebody as exposed in the western wall of a cross cut on 845 level (see Fig 6B, 7B).

Fig 10 Cross cutting relationships observed in core. A: olivine basalt intrusive into brecciated ultramafic, which has serpentinised reaction rims around the margins from drillhole MAD060; B and C: olivinite cross cutting altered gabbro in drillhole MAD189A, with clasts of gabbro contained within the olivinite; D: thin dyke of olivine basalt cutting poikilitic gabbro in drillhole MAD036; E: thin dykes of olivine basalt intruded into poikilitic gabbro showing magnetite reaction margins and angular clasts of sulfide and magnetite within the olivine basalt from drillhole MAD036.

Fig 11 A: Digital Elevation Model of Munali showing the outline of the intrusion, the gossans, the location of the drillhole collars and the downhole lithologies used the 3D modelling. B: 3D view of the modelled MUBU along the southwestern flank of the intrusive complex viewed towards the N. Potentially open zones at depth are marked in red; C: 3D view of the modelled MUBU viewed towards the NW to show the dip of the orebody. D: 3D view of the modelled MUBU viewed towards the NE to show the along strike variability. Note the potential open zones beneath Enterprise, Voyager and Intrepid.

Fig 12 Petrology of the igneous host rocks. A: microgabbro of the CGU; B: thin section (cross polarised light) of microgabbro made up of plagioclase (pl) with altered clinopyroxene (alt cpx) now chlorite and amphibole; C: poikilitic gabbro; D: thin section scan of coarse-grained poikilitic gabbro made up of plagioclase laths with oikocrystic clinopyroxene, altered to chlorite and amphiboles (alt cpx), and oikocrystic magnetite (mt). Note the much larger scale compared to the gabbro in B; E sulfide-bearing olivinite comprised of olivine (ol) with interstitial sulfide (sul) and magnetite: F: thin section (plane polarised light) of serpentinised olivinite showing olivine altered to serpentine (serp) with interstitial magnetite; G: pegmatoidal wehrlite made up of olivine and orthopyroxene (opx) and interstitial sulfide, magnetite and apatite (ap); H: phoscorite made up of coarse olivine and interstitial magnetite and apatite; I: thin section (plane polarised light) of olivine-magnetite rock; J: olivine basalt; K: thin section (plane polarised light) of olivine basalt showing plagioclase laths, highly altered clinopyroxene (alt cpx) and fully altered olivine phenocrysts (alt ol).

Fig 13 Sulfide styles and mineralogy of the Munali deposit. A: typical massive sulfide (sul) hosted breccia with clasts of olivinite (ol) and magnetite(mt)-olivine ultramafic (black/grey). Note sporadic pyrite (py); B: typical massive sulfide textures and mineralogy in reflected light, with abundant pyrrhotite (po) and minor pentlandite (pn), chalcopyrite (cpy), pyrite and coeval magnetite. Minor sulfide alteration by actinolite (act) is present; C: large (<20 cm) euhedral apatite (ap) hosted by massive sulfide-magnetite (sul-mt) in underground section; D: polished slab of apatite-magnetite-sulfide with small clasts of olivinite. Note the segregation of chalcopyrite from areas of massive pyrrohite-pentlandite; E: polished slab of talc-carbonate clast surrounded by massive sulfide; F: underground exposure of calcite-magnetite-sulfide vein showing euhedral calcite (cc) crystals and large calcite aggregates containing sulfide inclusions; G: thin section micrograph of a sulfide inclusions within calcite, shown in reflected light (to show opaque assemblage) and simultaneous transmitted light (to show calcite twinning); H: cut slab of poikilitic gabbro showing interstitial blebs of magmatic sulfide.

Fig 14 A: Layered image of poikilitic gabbro composed of plagioclase (pl) and altered oikocrystic clinopyroxene (alt cpx) and oxides shown in plane polarised light, with opaques and zircons colour coded using Mineralogic mapping and visualised in Atlas software. Inset image (C) shows zircons in plane polarised light (right) and backscattered electron imaging (left). B: Atlas layered image of phoscorite composed of serpentinised olivine (serp ol), magnetite, apatite and sulfides shown in plane polarised light, with opaques, apatite and zircons colour coded using Mineralogic mapping. Inset image (D) shows a zircon included in magnetite from the Mineralogic mapping (left) and in backscattered electron imaging (right); E: conchordia plot of $^{206}Pb/^{238}U$ ages for four zircons from poikilitic gabbro sample MAD36-155; F: conchordia plot of $^{206}Pb/^{238}U$ ages for four zircons from ultramafic phoscorite sample MAD36-155.

Fig 15 Summary of the Mesoproterozoic-early Palaeozoic geological history of southeast Zambia.

Table 1. Summary of electron microprobe analysis of olivines from the Munali ultramafic rocks.

Rock type	grains analysed	Fo content (mole%)			Ni content (ppm)		
		Max	Min	Mean	Max	Min	Mean
Olivinite	60	83.2	81.2	82.2	1154	11	610
Olivine-magnetite rock	45	77.5	74.6	76.5	1180	223	582
Pegmatitic wehrlite	43	75.2	78.8	76.8	1021	157	471

Table 2 U-Pb geochronology data from zircons from poikilitic gabbro (MAD-036-155) and phoscorite (MAD036-216).

	Compositional Parameters									Radiogenic Isotope Ratios								Isotopic Ages					
Sample	Wt. µg	U ppm	Pb ppm	Th/U	$^{206}Pb^*$ x10^{-13} mol	mol % $^{206}Pb^*$	Pb^*/Pb_c	Pb_c (pg)	$^{206}Pb/^{204}Pb$	$^{208}Pb/^{206}Pb$	$^{207}Pb/^{206}Pb$	% err	$^{207}Pb/^{235}U$	% err	$^{206}Pb/^{238}U$	% err	corr. coef.	$^{207}Pb/^{206}Pb$	±	$^{207}Pb/^{235}U$	±	$^{206}Pb/^{238}U$	±
MAD-036-155																							
A	9.1	42	6.6	0.658	2.2865	99.77%	138	0.44	8003	0.202	0.067962	0.258	1.340940	0.311	0.143102	0.167	0.561	867.38	5.35	863.64	1.81	862.18	1.35
B	1.7	36	6.3	0.856	0.3576	98.17%	18	0.55	1011	0.263	0.068237	0.818	1.352141	0.905	0.143714	0.279	0.451	875.76	16.93	868.48	5.28	865.63	2.26
C	2.8	42	6.7	0.608	0.6928	99.28%	43	0.41	2561	0.187	0.068178	0.479	1.345806	0.528	0.143165	0.197	0.424	873.98	9.91	865.75	3.07	862.53	1.59
D	1.9	61	10.4	0.872	0.7040	99.02%	34	0.57	1888	0.267	0.067702	0.826	1.336264	0.878	0.143149	0.272	0.341	859.46	17.14	861.61	5.10	862.44	2.19
F	0.8	95	16.2	0.837	0.4372	98.62%	24	0.50	1341	0.257	0.067754	0.783	1.337472	0.866	0.143169	0.243	0.466	861.03	16.25	862.13	5.03	862.56	1.96
MAD036-216																							
A	1.6	3	2.2	14.019	0.3011	98.20%	72	0.47	1026	4.367	0.069102	2.176	1.351685	2.314	0.141868	0.516	0.371	901.79	44.87	868.29	13.50	855.21	4.13
B	1.3	4	3.4	16.646	0.3384	98.23%	86	0.51	1047	5.108	0.067724	1.012	1.329431	1.121	0.142371	0.281	0.494	860.11	21.01	858.63	6.50	858.06	2.26
C	0.4	3	2.2	16.730	0.0648	90.14%	14	0.58	188	5.189	0.068882	3.752	1.356628	4.142	0.142841	1.102	0.471	895.21	77.45	870.42	24.21	860.71	8.88
F	1.0	10	10.1	21.656	0.0576	89.22%	16	0.57	172	6.586	0.067157	4.719	1.330697	4.853	0.143711	1.172	0.233	842.64	98.24	859.18	28.13	865.61	9.50

Fig 1

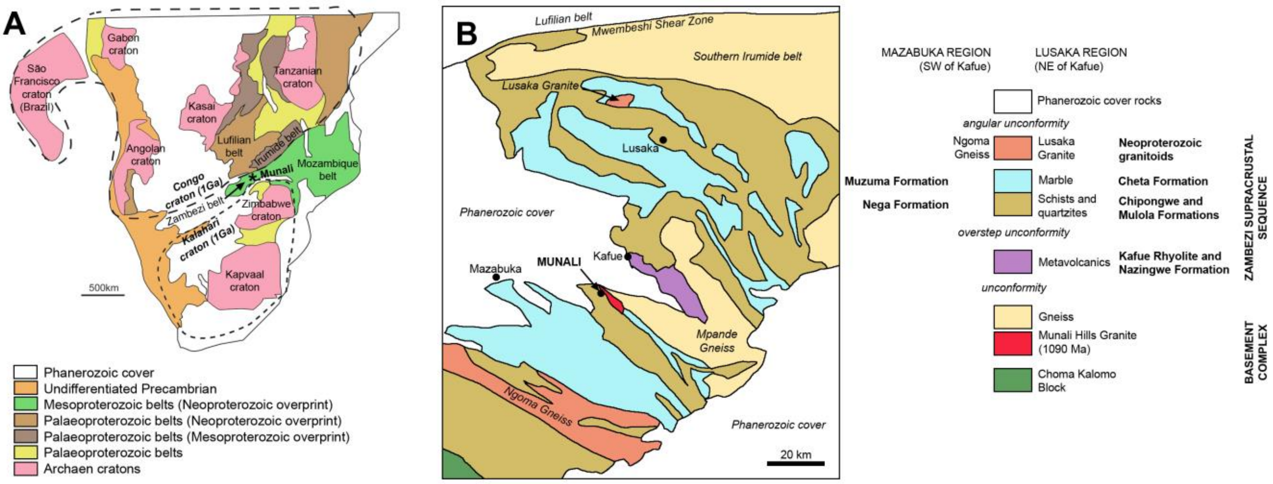
A
Gabon craton
São Francisco craton (Brazil)
Tanzanian craton
Kasai craton
Lufilian belt
Irumide belt
Angolan craton
Mozambique belt
Congo craton (1Ga)
Munali
Zambezi belt
Zimbabwe craton
Kalahari craton (1Ga)
Kapvaal craton
500km
Phanerozoic cover
Undifferentiated Precambrian
Mesoproterozoic belts (Neoproterozoic overprint)
Palaeoproterozoic belts (Neoproterozoic overprint)
Palaeoproterozoic belts (Mesoproterozoic overprint)
Palaeoproterozoic belts
Archaen cratons
B
Lufilian belt
Mwembeshi Shear Zone
Southern Irumide belt
Lusaka Granite
Lusaka
Phanerozoic cover
Kafue
MUNALI
Mazabuka
Mpande Gneiss
Ngoma Gneiss
Phanerozoic cover
20 km
MAZABUKA REGION (SW of Kafue)
LUSAKA REGION (NE of Kafue)
Phanerozoic cover rocks
angular unconformity
Ngoma Gneiss
Lusaka Granite
Neoproterozoic granitoids
Muzuma Formation
Marble
Cheta Formation
Nega Formation
Schists and quartzites
Chipongwe and Mulola Formations
ZAMBEZI SUPRACRUSTAL SEQUENCE
overstep unconformity
Metavolcanics
Kafue Rhyolite and Nazingwe Formation
unconformity
Gneiss
Munali Hills Granite (1090 Ma)
Choma Kalomo Block
BASEMENT COMPLEX

Fig 2

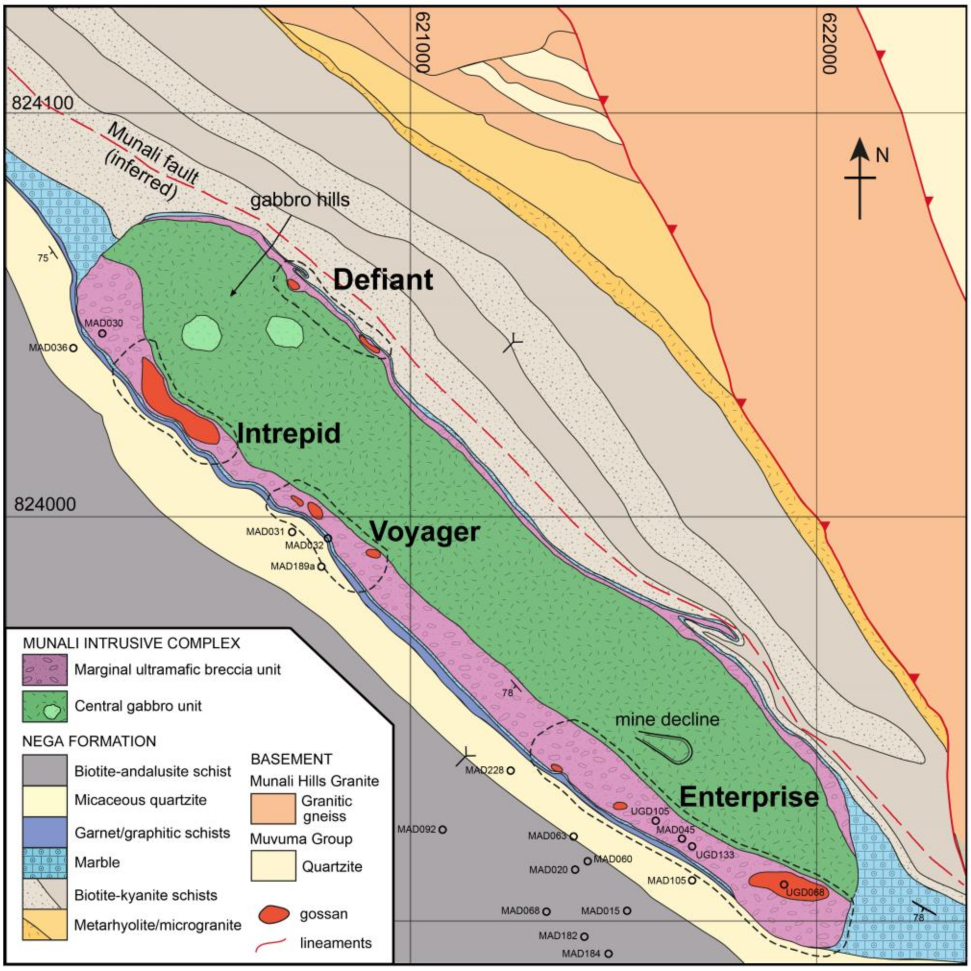
621000
622000
824100
824000
N
Munali fault
(inferred)
gabbro hills
Defiant
Intrepid
Voyager
Enterprise
mine decline
75
78
78
MAD030
MAD036
MAD031
MAD032
MAD189a
MAD228
MAD092
MAD063
MAD060
MAD020
UGD105
MAD045
UGD133
MAD105
UGD068
MAD068
MAD015
MAD182
MAD184
MUNALI INTRUSIVE COMPLEX
Marginal ultramafic breccia unit
Central gabbro unit
NEGA FORMATION
Biotite-andalusite schist
Micaceous quartzite
Garnet/graphitic schists
Marble
Biotite-kyanite schists
Metarhyolite/microgranite
BASEMENT
Munali Hills Granite
Granitic gneiss
Muvuma Group
Quartzite
gossan
lineaments

Fig 3

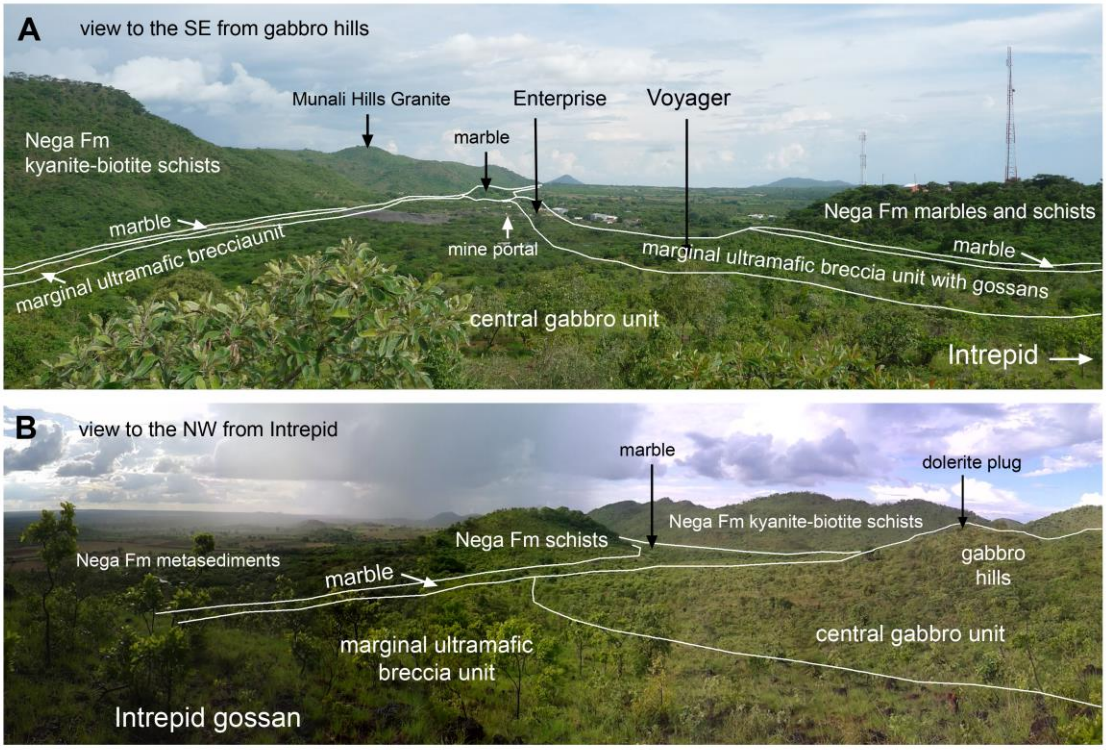

A
view to the SE from gabbro hills
Munali Hills Granite
Enterprise
Voyager
Nega Fm
kyanite-biotite schists
marble
marble
mine portal
Nega Fm marbles and schists
marble
marginal ultramafic brecciaunit
marginal ultramafic breccia unit with gossans
central gabbro unit
Intrepid
B
view to the NW from Intrepid
marble
dolerite plug
Nega Fm kyanite-biotite schists
Nega Fm schists
gabbro
hills
Nega Fm metasediments
marble
central gabbro unit
marginal ultramafic
breccia unit
Intrepid gossan

1466 Fig 4

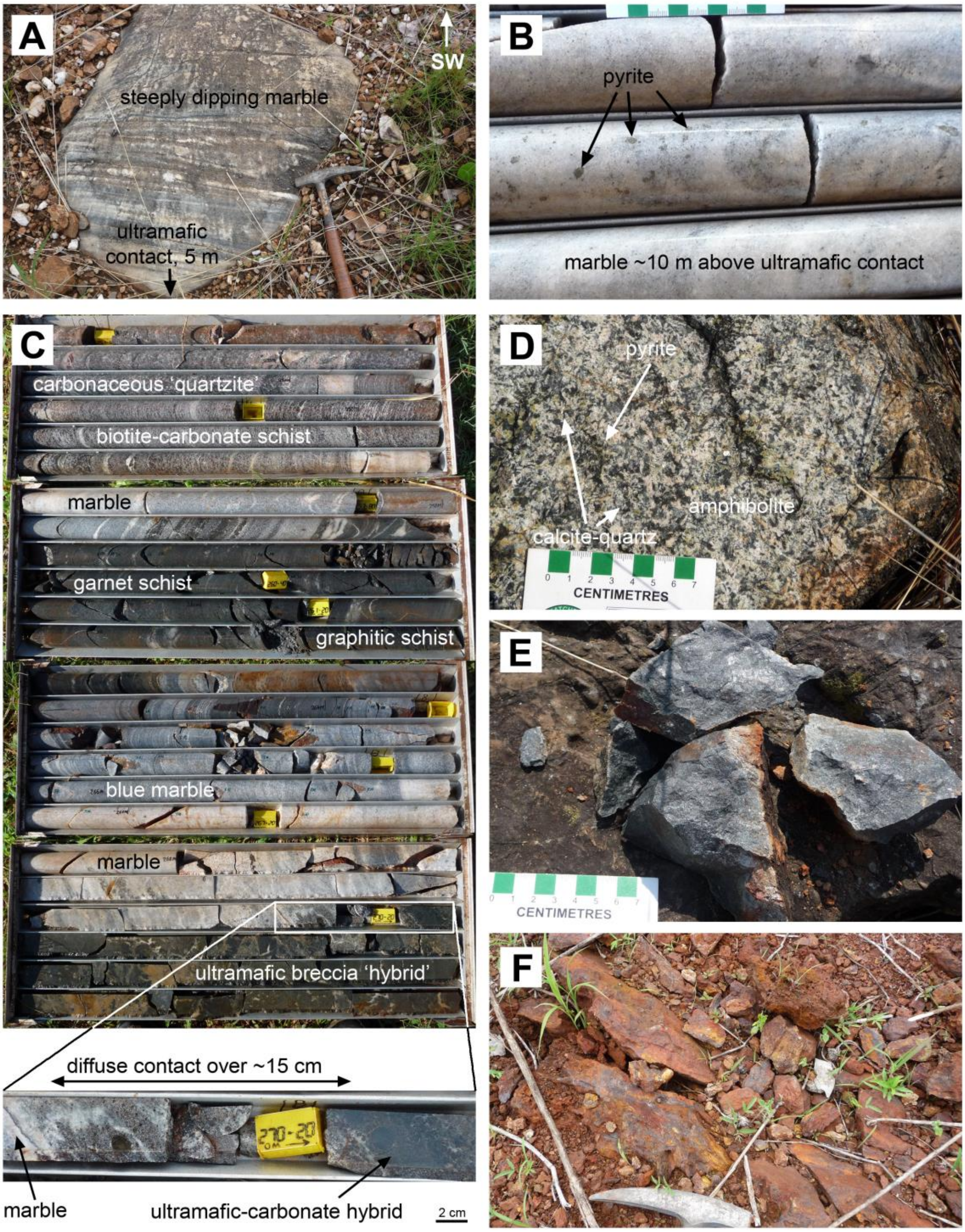

1467

1468

Fig 5

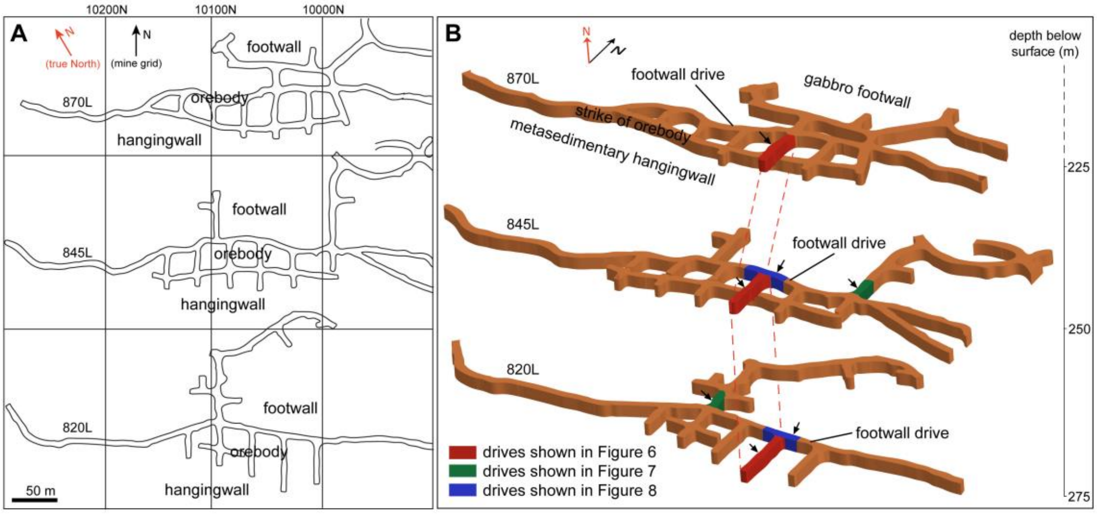
A
10200N
10100N
10000N
N
(true North)
N
(mine grid)
footwall
870L
orebody
hangingwall
footwall
845L
orebody
hangingwall
footwall
820L
orebody
hangingwall
50 m
B
N
N
depth below
surface (m)
870L
footwall drive
gabbro footwall
strike of orebody
metasedimentary hangingwall
225
845L
footwall drive
250
820L
footwall drive
drives shown in Figure 6
drives shown in Figure 7
drives shown in Figure 8
275

Fig 6

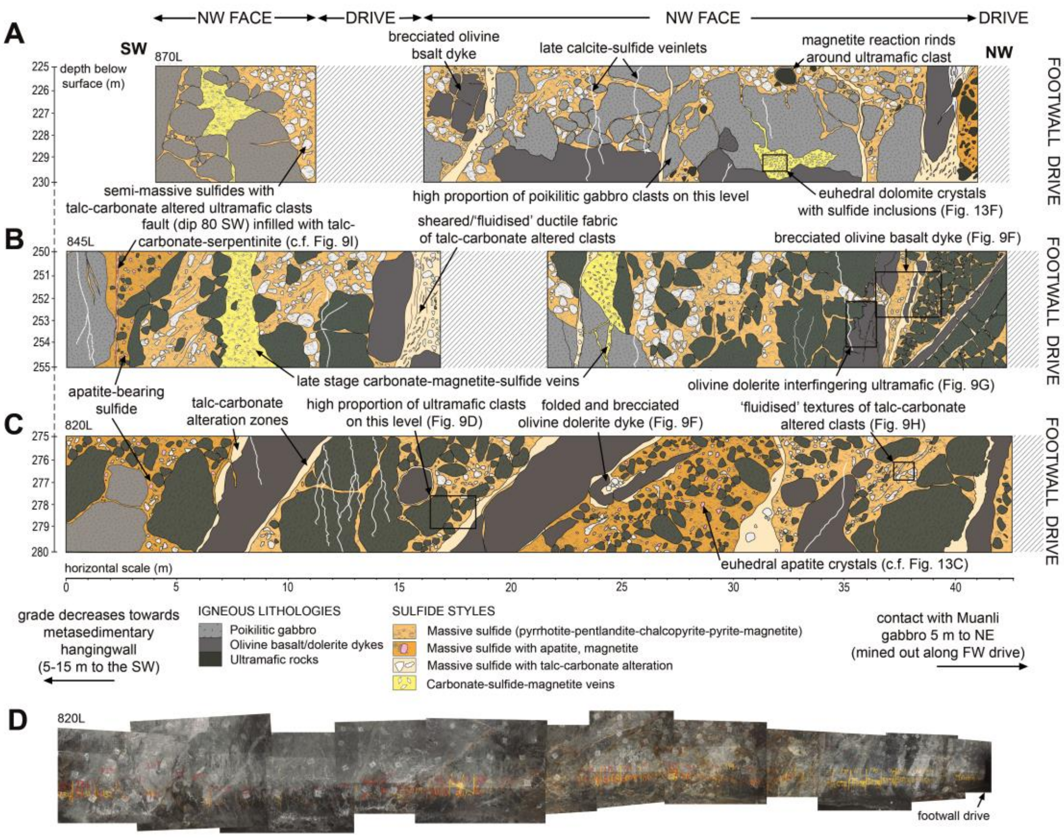

A
NW FACE
DRIVE
NW FACE
DRIVE
SW
NW
870L
225
226
227
228
229
230
depth below surface (m)
brecciated olivine bsalt dyke
late calcite-sulfide veinlets
magnetite reaction rinds around ultramafic clast
FOOTWALL DRIVE
semi-massive sulfides with talc-carbonate altered ultramafic clasts
high proportion of poikilitic gabbro clasts on this level
euhedral dolomite crystals with sulfide inclusions (Fig. 13F)
B
845L
250
251
252
253
254
255
fault (dip 80 SW) infilled with talc-carbonate-serpentinite (c.f. Fig. 9I)
sheared/'fluidised' ductile fabric of talc-carbonate altered clasts
brecciated olivine basalt dyke (Fig. 9F)
FOOTWALL DRIVE
apatite-bearing sulfide
late stage carbonate-magnetite-sulfide veins
olivine dolerite interfingering ultramafic (Fig. 9G)
C
820L
275
276
277
278
279
280
talc-carbonate alteration zones
high proportion of ultramafic clasts on this level (Fig. 9D)
folded and brecciated olivine dolerite dyke (Fig. 9F)
'fluidised' textures of talc-carbonate altered clasts (Fig. 9H)
FOOTWALL DRIVE
euhedral apatite crystals (c.f. Fig. 13C)
horizontal scale (m)
0
5
10
15
20
25
30
35
40
grade decreases towards metasedimentary hangingwall (5-15 m to the SW)
IGNEOUS LITHOLOGIES
Poikilitic gabbro
Olivine basalt/dolerite dykes
Ultramafic rocks
SULFIDE STYLES
Massive sulfide (pyrrhotite-pentlandite-chalcopyrite-pyrite-magnetite)
Massive sulfide with apatite, magnetite
Massive sulfide with talc-carbonate alteration
Carbonate-sulfide-magnetite veins
contact with Muanli gabbro 5 m to NE (mined out along FW drive)
D
820L
footwall drive

Fig 7

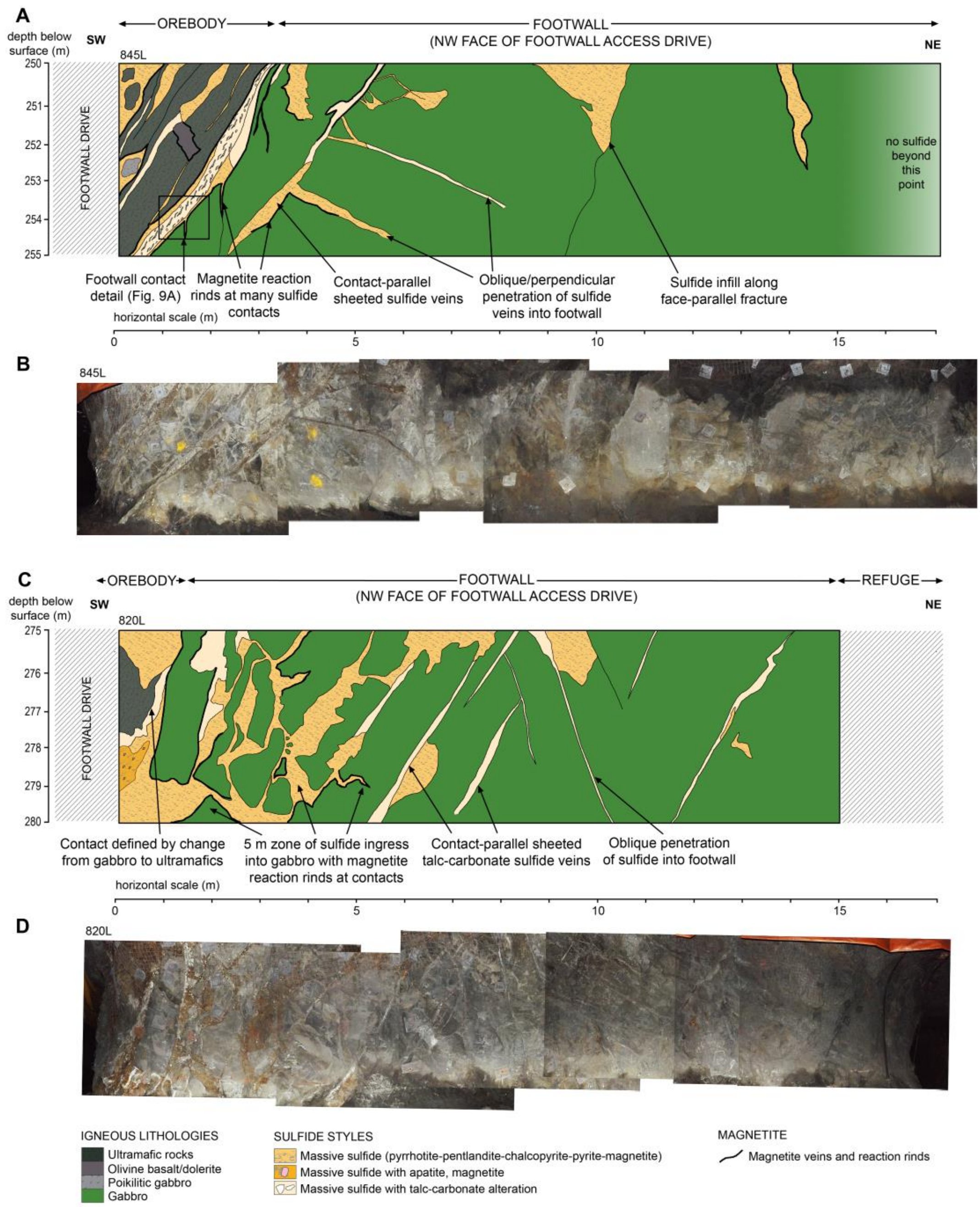
A
depth below surface (m)
SW
OREBODY
FOOTWALL
(NW FACE OF FOOTWALL ACCESS DRIVE)
NE
845L
250
251
252
253
254
255
FOOTWALL DRIVE
no sulfide beyond this point
Footwall contact detail (Fig. 9A)
Magnetite reaction rinds at many sulfide contacts
Contact-parallel sheeted sulfide veins
Oblique/perpendicular penetration of sulfide veins into footwall
Sulfide infill along face-parallel fracture
horizontal scale (m)
0
5
10
15
B
845L
C
depth below surface (m)
SW
OREBODY
FOOTWALL
(NW FACE OF FOOTWALL ACCESS DRIVE)
REFUGE
NE
820L
275
276
277
278
279
280
FOOTWALL DRIVE
Contact defined by change from gabbro to ultramafics
5 m zone of sulfide ingress into gabbro with magnetite reaction rinds at contacts
Contact-parallel sheeted talc-carbonate sulfide veins
Oblique penetration of sulfide into footwall
horizontal scale (m)
0
5
10
15
D
820L
IGNEOUS LITHOLOGIES
Ultramafic rocks
Olivine basalt/dolerite
Poikilitic gabbro
Gabbro
SULFIDE STYLES
Massive sulfide (pyrrhotite-pentlandite-chalcopyrite-pyrite-magnetite)
Massive sulfide with apatite, magnetite
Massive sulfide with talc-carbonate alteration
MAGNETITE
Magnetite veins and reaction rinds

Fig 8

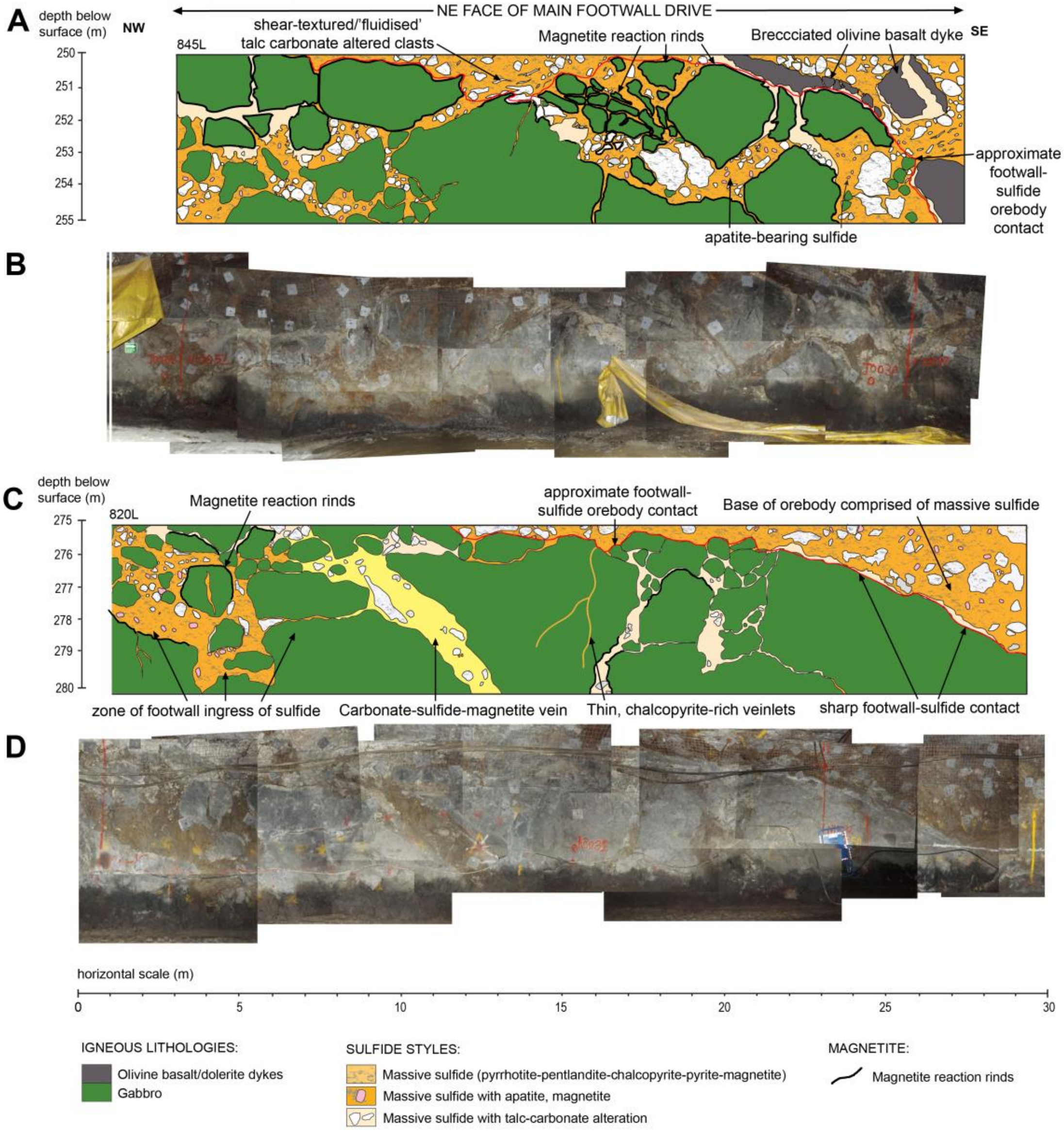

A
depth below surface (m)
NW
NE FACE OF MAIN FOOTWALL DRIVE
SE
845L
250
251
252
253
254
255
shear-textured/'fluidised' talc carbonate altered clasts
Magnetite reaction rinds
Brecciated olivine basalt dyke
approximate footwall-sulfide orebody contact
apatite-bearing sulfide
B
C
depth below surface (m)
820L
275
276
277
278
279
280
Magnetite reaction rinds
approximate footwall-sulfide orebody contact
Base of orebody comprised of massive sulfide
zone of footwall ingress of sulfide
Carbonate-sulfide-magnetite vein
Thin, chalcopyrite-rich veinlets
sharp footwall-sulfide contact
D
horizontal scale (m)
0
5
10
15
20
25
30
IGNEOUS LITHOLOGIES:
Olivine basalt/dolerite dykes
Gabbro
SULFIDE STYLES:
Massive sulfide (pyrrhotite-pentlandite-chalcopyrite-pyrite-magnetite)
Massive sulfide with apatite, magnetite
Massive sulfide with talc-carbonate alteration
MAGNETITE:
Magnetite reaction rinds

Fig 9

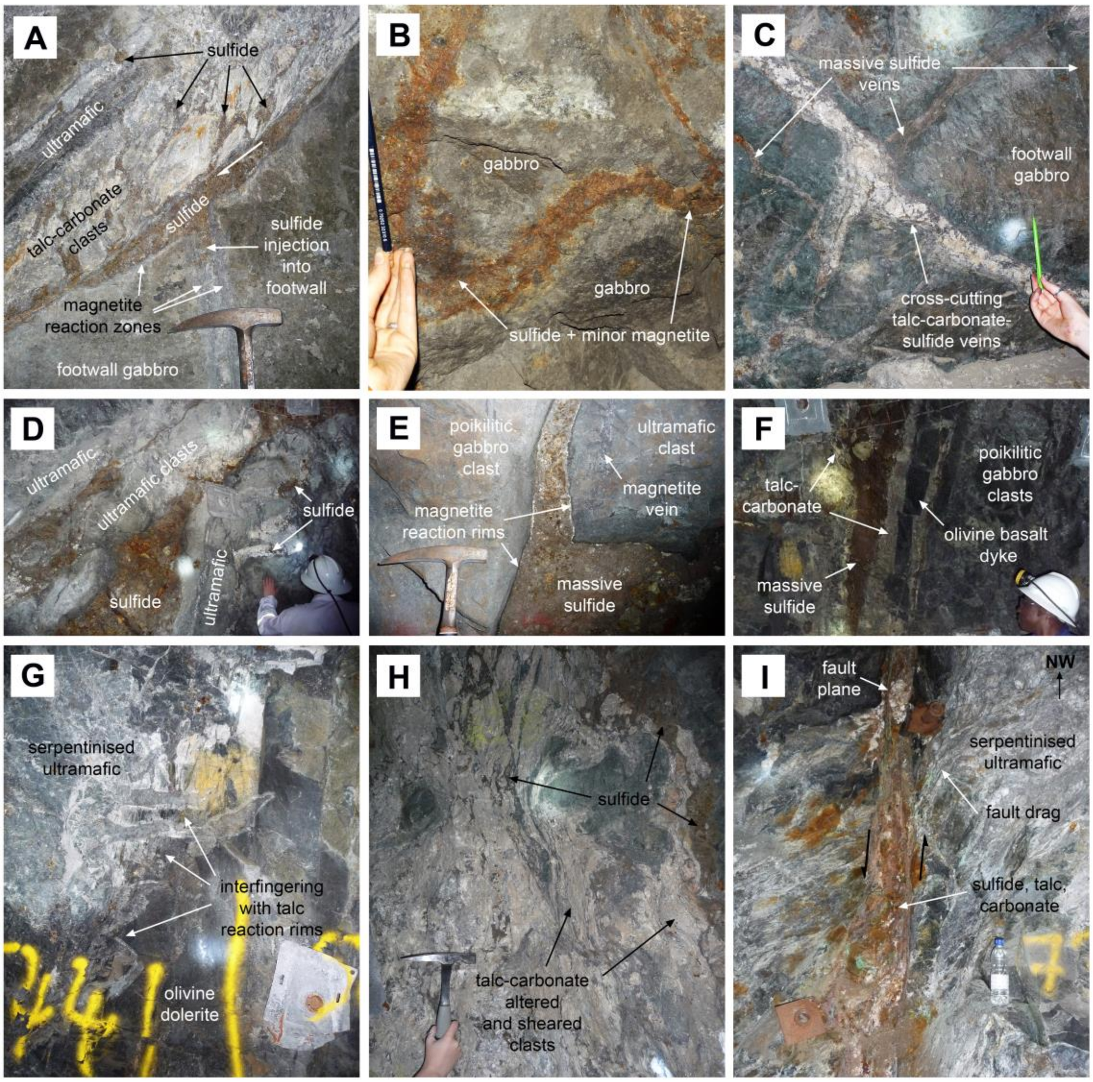
A
sulfide
ultramafic
talc-carbonate clasts
sulfide
sulfide injection into footwall
magnetite reaction zones
footwall gabbro
B
gabbro
gabbro
sulfide + minor magnetite
C
massive sulfide veins
footwall gabbro
cross-cutting talc-carbonate-sulfide veins
D
ultramafic
ultramafic clasts
sulfide
sulfide
ultramafic
E
poikilitic gabbro clast
ultramafic clast
magnetite vein
magnetite reaction rims
massive sulfide
F
talc-carbonate
poikilitic gabbro clasts
olivine basalt dyke
massive sulfide
G
serpentinised ultramafic
interfingering with talc reaction rims
olivine dolerite
H
sulfide
talc-carbonate altered and sheared clasts
I
fault plane
NW
serpentinised ultramafic
fault drag
sulfide, talc, carbonate

Fig 10

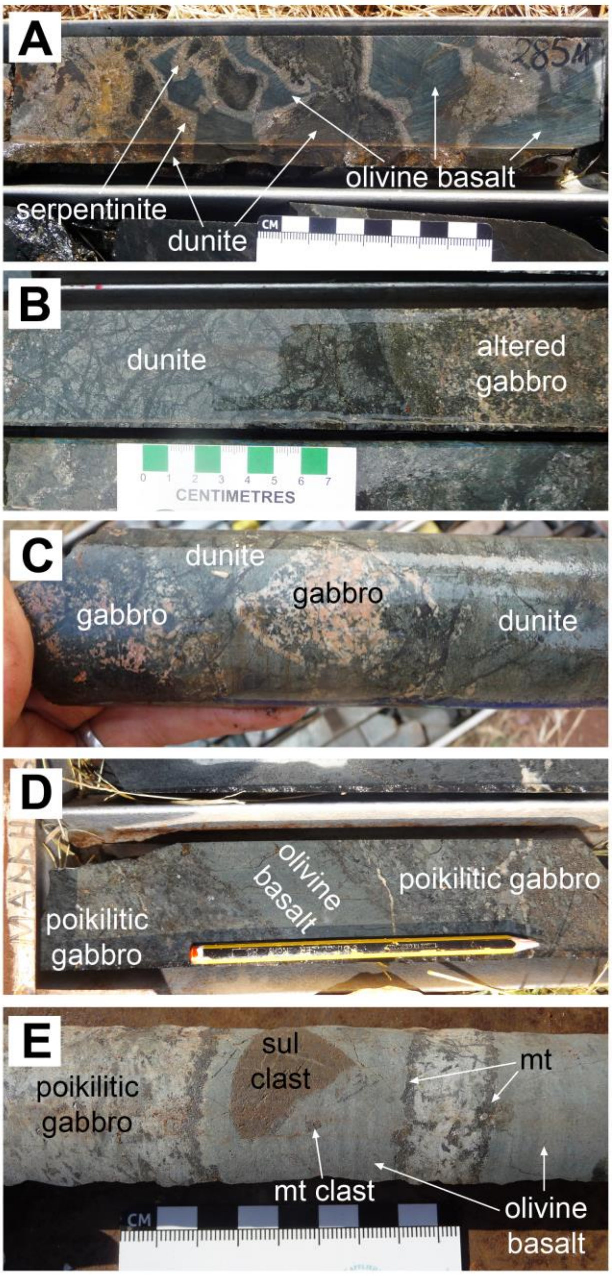
A
285M
olivine basalt
serpentinite
dunite
CM
B
dunite
altered
gabbro
CENTIMETRES
C
dunite
gabbro
gabbro
dunite
D
olivine
basalt
poikilitic gabbro
poikilitic
gabbro
E
sul
clast
mt
poikilitic
gabbro
mt clast
olivine
basalt
CM

Fig 11

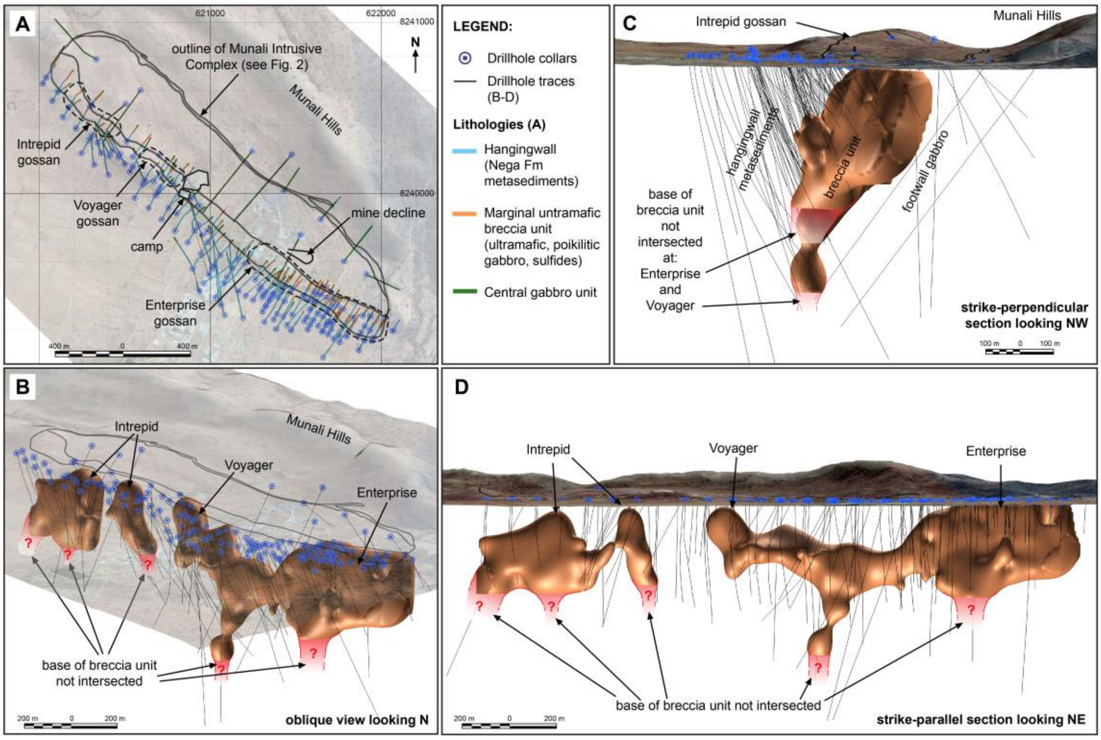
A
621000
622000
8241000
8240000
N
outline of Munali Intrusive Complex (see Fig. 2)
Munali Hills
Intrepid gossan
Voyager gossan
camp
mine decline
Enterprise gossan
LEGEND:
Drillhole collars
Drillhole traces (B-D)
Lithologies (A)
Hangingwall (Nega Fm metasediments)
Marginal untramafic breccia unit (ultramafic, poikilitic gabbro, sulfides)
Central gabbro unit
C
Intrepid gossan
Munali Hills
hangingwall metasediments
breccia unit
footwall gabbro
base of breccia unit not intersected at: Enterprise and Voyager
strike-perpendicular section looking NW
B
Intrepid
Voyager
Enterprise
Munali Hills
base of breccia unit not intersected
oblique view looking N
D
Intrepid
Voyager
Enterprise
base of breccia unit not intersected
strike-parallel section looking NE

Fig 12

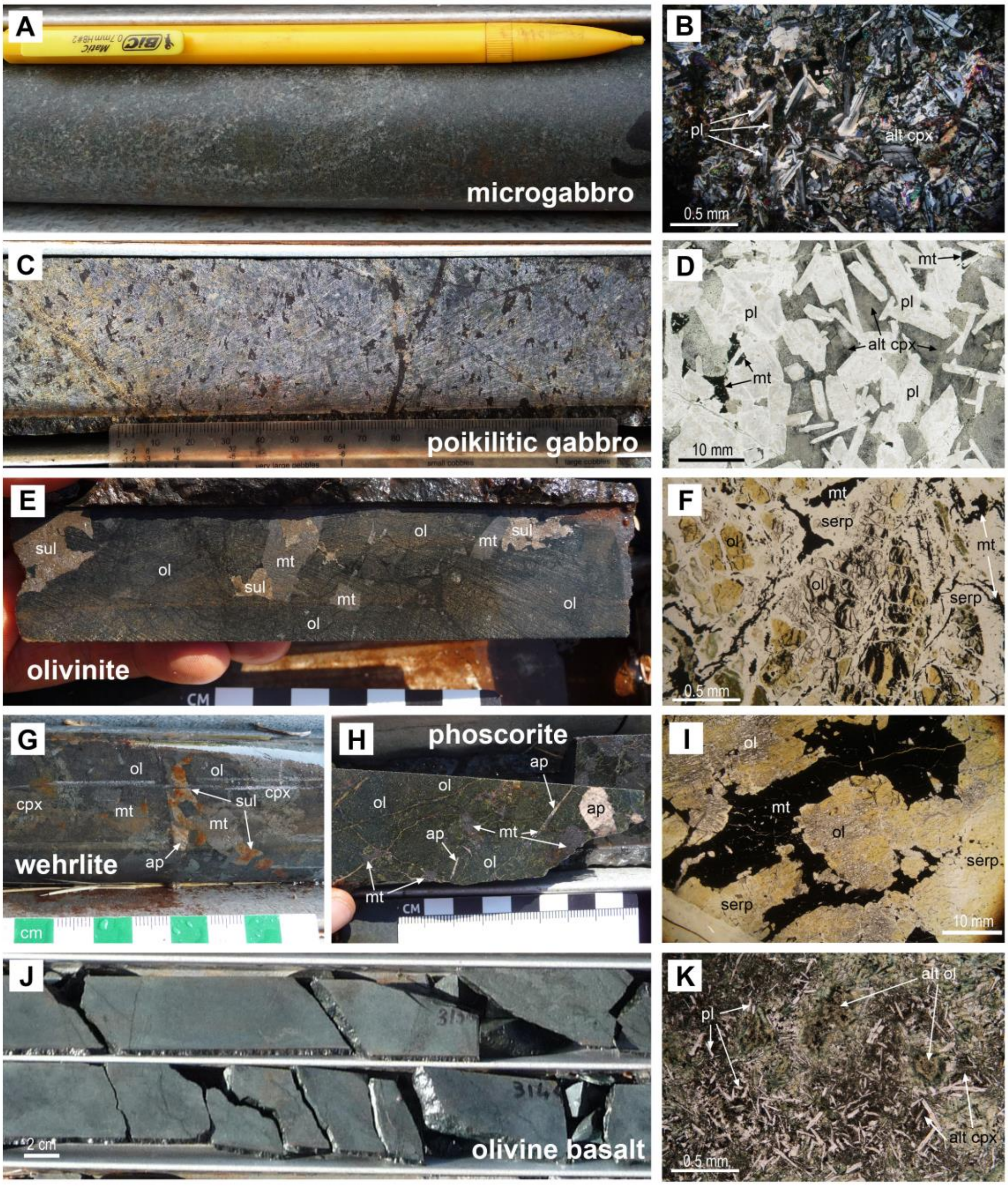

A
microgabbro
B
pl
alt cpx
0.5 mm
C
poikilitic gabbro
D
mt
pl
alt cpx
10 mm
E
sul
ol
mt
olivinite
CM
F
mt
serp
ol
0.5 mm
G
ol
cpx
mt
sul
ap
wehrlite
cm
H
phoscorite
ap
ol
mt
CM
I
ol
mt
serp
10 mm
J
2 cm
olivine basalt
K
alt ol
pl
alt cpx
0.5 mm

1493 Fig 13

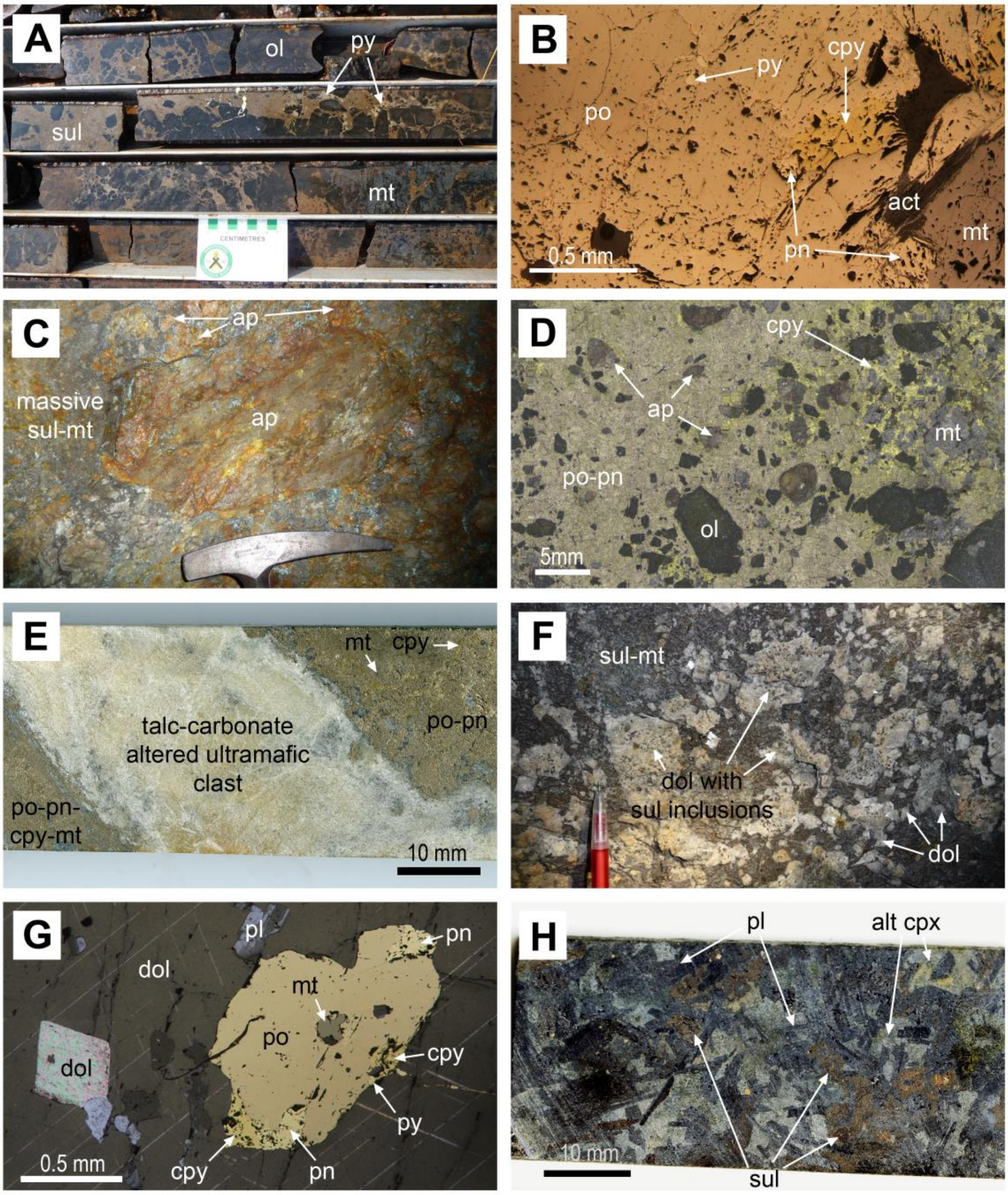

1494

1495

Fig 14

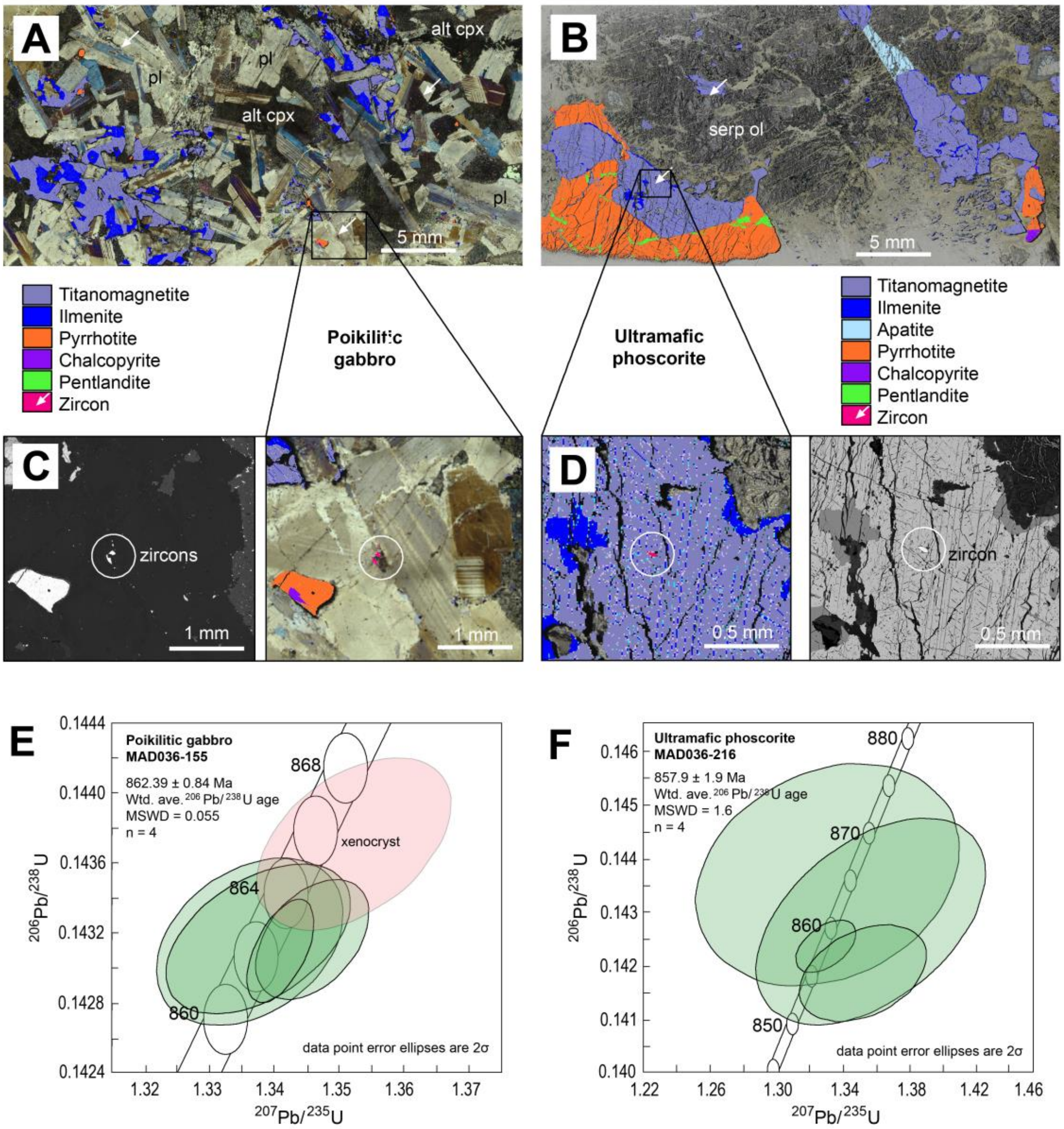
A
alt cpx
pl
alt cpx
pl
5 mm
B
serp ol
5 mm
Titanomagnetite
Ilmenite
Pyrrhotite
Chalcopyrite
Pentlandite
Zircon
Poikilitic gabbro
Ultramafic phoscorite
Titanomagnetite
Ilmenite
Apatite
Pyrrhotite
Chalcopyrite
Pentlandite
Zircon
C
zircons
1 mm
1 mm
D
0.5 mm
zircon
0.5 mm
E
Poikilitic gabbro
MAD036-155
862.39 ± 0.84 Ma
Wtd. ave. 206Pb/238U age
MSWD = 0.055
n = 4
868
xenocryst
864
860
data point error ellipses are 2σ
206Pb/238U
207Pb/235U
F
Ultramafic phoscorite
MAD036-216
857.9 ± 1.9 Ma
Wtd. ave. 206Pb/238U age
MSWD = 1.6
n = 4
880
870
860
850
data point error ellipses are 2σ
206Pb/238U
207Pb/235U

1499 Fig 15

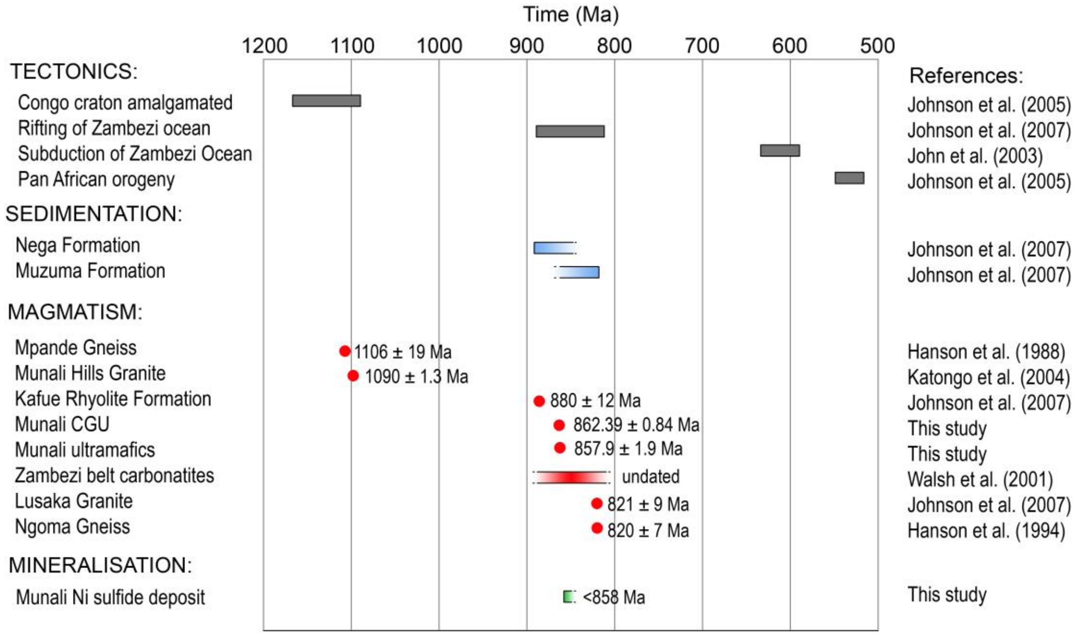

1500